NONLINEAR SEISMIC ANALYSIS USING VECTOR SUPERPOSITION METHODS

by

Serge Dussault

Department of Civil Engineering and Applied Mechanics McGill University, Montreal May, 1991

A thesis submitted to the Faculty of Graduate Studies and Research in partial fulfilment of the requirements for the degree of Master of Engineering

ABSTRACT

Nonlinear dynamic analysis of MDOF structures is usually performed in geometric coordinates using a step-by-step integration of all modes simultaneously. The mode superposition used extensively in linear problems can be thought competitive and efficient in nonlinear problems if a truncated vector basis can be considered.

This thesis presents two algorithms to solve nonlinear seismic problems in generalized coordinates, one that uses a set of vectors computed from initial properties, the Pseudo-Force Method (PFM), and another that continuously updates the vector basis to represent the nonlinear behaviour, the Tangent Spectrum Method (TSM). Both methods can use either exact eigenvectors or load dependent vectors as vector basis. Parametric analyses are carried out on a series of multistory buildings idealized as shear beam structures with bilinear hysteretic behaviour. The effects of the truncation of the vector basis on the stability and the quality of the nonlinear solutions are investigated using nonlinear response parameters such as ductility, energy balance, and dissipation. The algorithms are then used to make a comparative study on the effects of different mathematical representations of viscous damping based either on initial elastic, or tangent modal, properties of MDOF structures.

For a flexible 25-story structure, the solution is much more sensitive to the truncation of the vector basis when the PFM is used instead of the TSM. However, even if the TSM yields accurate g, ball results based on displacements such as ductility and hysteretic energy dissipation, it shows important error in velocity and acceleration when a small number of vectors is used. For a stiff 5-story structure, the trend is reversed and the PFM seems to be more accurate when a truncated basis is used. The equilibrium iterations are found to be very important to reduce the required number of basis updates in the TSM algorithm. The use of eigenvectors or load dependent vectors yielded comparable results. A tangent Rayleigh damping model that maintains a constant damping ratio throughout the elastic and inelastic response has been developed. If initial elastic vectors are used, a very good approximation to the rigorous response based on tangent damping is obtained from damping proportional to the instantaneous stiffness for MDOF structures with fundamental periods of vibration, $T_1 \leq 0.5$ sec. For structures with $T_1 > 0.5$ sec, Rayleigh damping based on initial elastic properties should be used.

RÉSUMÉ

Une analyse dynamique d'un système non-linéaire à plusieurs degrés de liberte est habituellement résolue en utilisant l'intégration pas- .-pas de tous les modes simultanément. La méthode de superposition modale, utilisée pour les problèmes linéaires, peut possiblement être compétitive et efficace pour un problème non-linéaire si une base de vecteurs tronquée peut être considérée.

Cette thèse présente deux algorithmes pour résoudre des problèmes séismiques nonlinéaires en coordonnées généralisées. Le premier utilise un ensemble de vecteurs calculés à
partir des propriétés initiales (Méthode de Pseudo-Force, MPF), et l'autre met à jour la base de
vecteurs pour représenter le comportement non-linéaire (Méthode du Spectre Tangent, MST).
Les deux méthodes utilisent soit des vecteurs propres ou vecteurs dépendants de la charge
comme base vectorielle. Des études paramétriques sont menées sur une série de bâtiments
multi-étagés idéalisés par des poutres de cisaillement à deux degrés de liberté avec
comportement bi-linéaire hystérétique. Les effets de la troncation de la base vectorielle sur la
stabilité et la qualité de la solution non-linéaire sont examinés en utilisant des indicateurs tels
que la ductilité, la balance et la dissipation d'énergie. Les algorithmes sont ensuite utilisés pour
mener une étude comparative sur les effets de différents modèles de matrices d'amortissement
calculées soit à partir des propriétés initiales ou tangentes du système.

Pour un bâtiment flexible de 25 étages, la troncation de la base vectorielle est beaucoup plus sensible pour la MPF que la MST. Cependant, même si la MST donne des résultats globaux satisfaisants, elle produit des erreurs considérables dans les vecteurs vitesse et accélération quand un nombre peu élevé de vecteurs est utilisé. Pour un bâtiment rigide de 5 étages, la tendance est renversée et la MPF semble plus précise. Les itérations d'équilibre sont très importantes pour faire de la MST un algorithme intéressant et compétitif. L'utilisation de vecteurs propres ou de vecteurs dépendants de la charge donne des résultats comparables. Un modèle d'amortissement tangent qui maintient un taux d'amortissement constant au cours d'une analyse non-linéaire a été développé. Si les vecteurs initiaux élastiques sont utilisés, une très bonne approximation de la réponse rigoureuse basée sur l'amortissement tangent est obtenue à partir de l'amortissement proportionnel à la rigidité instantanée pour structures à plusieurs degrés de liberté avec périodes fondamentales de vibration, $T_1 \leq 0.5$ sec. Pour les structures avec $T_1 > 0.5$ sec., l'amortissement de type Rayleigh, basé sur les propriétés initiales élastiques, devrait être utilisé.

ACKNOWLEDGEMENTS

The author would like to thank Professor Pierre Léger for his support, assistance and all his suggestions and comments made through a friendly relationship. This research has been made possible through the support given by the * Fonds pour la Formation de Chercheurs et l'Aide à la Recherche*. The financial support given through the Engli Nenniger Memorial Fellowship was also greatly appreciated.

Finally, the author would like to mention the constant support and the encouragement given to him by his family ,friends and especially his wife.

TABLE OF CONTENTS

ABSTRACT
RÉSUMÉ
ACKNOWLEDGEMENTS III
TABLE OF CONTENTS
LIST OF FIGURES vii
LIST OF TABLES ix
CHAPTER 1
INTRODUCTION 1
1.1 OVERVIEW AND OBJECTIVES 1
1.2 REVIEW OF PAST WORK
1.3 SCOPE OF THE PRESENT STUDY
CHAPTER 2
SOLUTION STRATEGIES FOR NONLINEAR DYNAMIC ANALYSIS 7
2.1 SOURCES OF NONLINEARITIES
2.2 EQUATION OF DYNAMIC EQUILIBRIUM
2.3 VECTOR SUPERPOSITION IN NONLINEAR DYNAMIC ANALYSIS
2.3.1 Pseudo-Force Method (PFM)
2.3.2 Tangent Spectrum Method (TSM)
2.4 SELECTION OF VECTOR BASIS
2.5 COMPUTER IMPLEMENTATION OF NONLINEAR SOLUTION
ALGORITHMS
CHAPTER 3
INDICATORS TO CHARACTERIZE NONLINEAR BEHAVIOUR 19
3.1 EVOLUTION OF TANGENT MODAL PROPERTIES
3.2 DISPLACEMENT DUCTILITY
3.3 ENERGY INDICATORS
3.3.1 Energy balance
3.3.2 Energy dissipation
3.3.3 Rate of energy dissipation, power 23
2.4 VIELDING SECHENCE

CHAPTER 4 SYSTEMS ANALYSED 25 4.1 STRUCTURAL MODELS 25 4.1.1 Element action-deformation model 25 4.1.2 Design procedure 25 4.1.3 Structural properties 27 4.2 EARTHQUAKE LOADING 29 4.2.1 Selected earthquakes 29 4.2.2 Scaling method 29 CHAPTER 5 NONLINEAR SEISMIC RESPONSE USING VECTOR SUPERPOSITION 33
4.1 STRUCTURAL MODELS 25 4.1.1 Element action-deformation model 25 4.1.2 Design procedure 25 4.1.3 Structural properties 27 4.2 EARTHQUAKE LOADING 29 4.2.1 Selected earthquakes 29 4.2.2 Scaling method 29
4.1.1 Element action-deformation model 25 4.1.2 Design procedure 25 4.1.3 Structural properties 27 4.2 EARTHQUAKE LOADING 29 4.2.1 Selected earthquakes 29 4.2.2 Scaling method 29
4.1.2 Design procedure 25 4.1.3 Structural properties 27 4.2 EARTHQUAKE LOADING 29 4.2.1 Selected earthquakes 29 4.2.2 Scaling method 29
4.1.3 Structural properties 27 4.2 EARTHQUAKE LOADING 29 4.2.1 Selected earthquakes 29 4.2.2 Scaling method 29 CHAPTER 5
4.2 EARTHQUAKE LOADING 29 4.2.1 Selected earthquakes 29 4.2.2 Scaling method 29 CHAPTER 5
4.2.1 Selected earthquakes 29 4.2.2 Scaling method 29 CHAPTER 5
4.2.2 Scaling method
CHAPTER 5
5.1 TANGENT SEISMIC RESPONSE ANALYSIS
5.1.1 Evolution of tangent modal properties
5.1.2 Performance of tangent solution
5.2 EFFECTS OF VECTOR BASIS TRUNCATION
5.2.1 Convergence of nonlinear response indicators - 25-story
building
5.2.2 Convergence of nonlinear response indicators - 5-story building 42
5.3 CONCLUSIONS
CHAPTER 6
MATHEMATICAL MODELS FOR VISCOUS DAMPING
6.1 INFLUENCE OF VISCOUS DAMPING ON ENERGY ABSORPTION 47
6.2 DAMPING MATRIX FORMULATION 48
CHAPTER 7
SEISMIC ENERGY DISSIPATION IN MDOF STRUCTURES
7.1 INTRODUCTION
7.2 INFLUENCE OF DAMPING MODELS ON SEISMIC RESPONSE
7.2.1 Evolution of nonlinear tangent properties
7.2.2 Displacement responses at the top
7.2.3 Nonlinear response indicators
7.3 PARAMETRIC STUDY

7.3.1 Influence of damping ratio 61

7.3.2	Influence of force reduction factor	62
7.3.3 1	Influence of strain hardening ratio	64
7.4 CONCLUS	SIONS	66
CHAPTER 8		
CONCLUSIONS		69
8.1 SUMMARY	Y	69
8.2 CONCLUS	SIONS	71
8.2.1	Vectors superposition methods	71
8.2.2	Mathematical modelling of viscous damping	72
8.3 RECOMM	ENDATIONS FOR FURTHER STUDIES	73
REFERENCES		7.1

LIST OF FIGURES

Figure 2.1.	Sources of nonlinearities.	8
Figure 2.2.	Action-deformation model of structural elements.	9
Figure 2.3.	Rate of convergence of tangent and pseudo-force methods.	11
Figure 4.1.	NBC pseudo-static earthquake loading distribution.	26
Figure 4.2.	Selected earthquakes.	30
Figure 4.3.	Scaled Earthquake spectra.	31
Figure 5.1.	Input motion and evolution of tangent modal properties for 25-story building. (a) El Centro accelerogram. (b) Evolution of fundamental period, T ₁ . (c) No. of modes for 95% of effective modal mass.	35
Figure 5.2.	Performance of Tangent Spectrum Method for 25-story building. (a) Effect of computing acceleration vector from the condition of dynamic equilibrium at time $t+\Delta t$. (b) Ductility demand for solution without equilibrium iteration. (c) Ductility demand for solution with equilibrium iterations.	36
Figure 5.3.	Time-history of displacement and force responses for the 25-story building using the TSM-LDM with 25, 11, and 5 vectors.	39
Figure 5.4.	Effect of the number of transformation vectors on the peak ductility demand in each story for different solution strategies - 25-story building.	40
Figure 5.5.	Convergence of various nonlinear response indicators for different solution strategies - 25-story building.	42
Figure 5.6.	Effect of the number of transformation vectors on the peak ductility demand in each story for different solution strategies - 5-story building.	43
Figure 5.7.	Convergence of various nonlinear response indicators for different solution strategies - 5-story building.	44

Figure 6.1.	Fayleigh damping.	50
Figure 7.1.	Evolution of tangent modal properties using damping model M3(a,b) for the 10-story building subjected to El Centro earthquake (R=4, α =1%, ξ =5%), a) period of the first mode, b) number of modes for 95% of effective modal mass	55
Figure 7.2.	Evolution of the Rayleigh damping coefficients using damping model M3(a, b,) for the 10-story building subjected to the El Centro earthquake (R=4, α =1%, ξ =5%)	56
Figure 7.3.	Top displacement of the 10-story building subjected to the El Centro earthquake for various damping models (R=4, α =1%, ξ =5%)	57
Figure 7.4.	Nonlinear response indicators for the 10-story building for various damping models (R=4, α =1%, ξ =5%).	59
Figure 7.5.	Power response indicators for the 10-story building for various damping models (R=4, α =1%, ξ =5%).	60
Figure 7.6.	Influence of the damping ratio, ξ , on the response of multistory buildings (R=4, α =1%) subjected to the El Centro earthquake	63
Figure 7.7.	Influence of the force modification factor, R, on the response of multistory buildings (ξ =5%, α =1%) subjected to the El Ceritro earthquake.	65
Figure 7.8.	Influence of the strain hardening ratio, α , on the response of multistory buildings (R=4, ξ =5%) subjected to the El Centro earthquake.	67

LIST OF TABLES

Table 2.1.	Pseudo-Force Method (PFM).	13
Table 2.2.	Tangent Spectrum Method (TSM).	16
Table 2.3.	Load dependent vectors (LD).	18
Table 4.1.	Properties of structures analyzed.	28
Table 4.2.	Strength parameter, η , of structures analyzed for R=4.	28
Table 4.3.	Scaling factors for the earthquake records.	32
Table 5.1.	Effects of equilibrium iterations and time-step on the number of basis updates.	37

CHAPTER 1

INTRODUCTION

1.1 OVERVIEW AND OBJECTIVES

It is generally recognized that it is uneconomical to design all building structures to remain in the elastic range to resist major earthquakes. Step-by-step integration of the incremental form of the equations of dynamic equilibrium expressed in geometric coordinates is generally used to investigate the nonlinear seismic behaviour of MDOF structures. The integration procedure mathematically corresponds to the simultaneous integration of all instantaneous modes of vibration using the same time-step. The use of vector superposition methods in nonlinear analysis consists in performing a change of basis to a more effective system of equation. The effectiveness of vector superposition techniques in nonlinear dynamic problems depends on (i) the number of vectors required to simulate accurately the response, (ii) the frequency of updating and recalculating the basis vectors, which are a function of the rate of change of these vectors with time, and (iii) the efficiency of the algorithm used to calculate the initial vectors and updating them (Noor 1981). Vector superposition methods in nonlinear structural dynamics can be based on either the Tangent Spectrum Method (TSM) (Maison and Kasai 1990, Ibrahimbegovic and Wilson 1990, Idelsohn and Cardona 1985, Gillies and Shepherd 1983, Remseth 1979, Nickell 1976) or the Pseudo-Force Method (PFM) (Chang and Moraz 1990, Muscolino 1989, Hanna 1989, Filho et al. 1988, Knight 1985, Dungar 1982, Bathe and Gracewski 1981, Geschwindner 1981, Lukkunaprasit et al. 1980, Shah et al. 1979, Clough and Wilson 1979, Hofmeister 1978, Morris 1977, Stricklin and Haisler 1977, Molnar et al. 1976). In the TSM, the change of basis is performed at each time-step using vector shapes and frequencies corresponding to the instantaneous system matrices. In the PFM, a single set of vectors, based on linear system matrices, is used throughout the analysis. The linear system matrices are employed during the complete response calculation, and the nonlinearities are taken as pseudoforces on the right hand side of the equations of motion. The PFM avoids the solution of the tangent eigenproblem at each time-step during nonlinear behaviour, and has been found to be competitive regarding computational effort with direct integration operators in geometric coordinates in numbers of simple nonlinear structural dynamic problems.

The satisfactory seismic performance of structures designed to reduced elastic strength demand according to modern building codes, has been mainly attributed to overstrength and dynamic response modification in the inelastic range, corresponding to changes in period of vibration, effective damping, and related energy dissipation mechanisms. The TSM provides knowledge of the spectrum of frequencies for the dominating modes throughout the inelastic seismic response. This present several potential advantages such as:

- (i) A rationalization of nonlinear behaviour in an elastic format to evaluate period elongations, and Rayleigh damping matrices based on tangent modal properties.
- (ii) A better representation of the inertia forces in inelastic configuration using instantaneous mode shapes instead of the elastic deformation modes used in the PFM.
- (iii) A mean to develop simplified seismic design methodology based on modified elastic modal response as given in building codes (Lin and Mahin 1985, Villaverde 1988).
- (iv) The definition of new damage indices based on the evolution of tangent modal properties during the earthquake (DiPasquale et al. 1990).
- (v) A direct control on the participation of higher modes that can be explicitly excluded of the solution instead of relying on numerical damping.

The objectives of this thesis are to develop proper solution strategies for nonlinear seismic analysis using generalized coordinates, and to investigate the effects of different mathematical representations of viscous damping on nonlinear response parameters such as: energy, power, ductility, and number of yield excursions. In the first part of this study, different solution strategies to solve nonlinear seismic problems are investigated with an emphasis on the effect of the retained strategy (PFM or TSM), modal truncation, and basis vector selection. The second part focuses on energy loss mechanisms in nonlinear seismic analysis. The effect of different modelling procedures for viscous damping on nonlinear response parameters is assessed.

1.2 REVIEW OF PAST WORK

Previous investigations related to inelastic seismic analyses of MDOF structures using vector superposition methods, have been almost exclusively based on the PFM. Lukkunaprasit (1980) analyzed a 30-story shear building subjected to an amplified NS component of the 1940 El Centro Earthquake. It was concluded that the PFM was able to predict accurately the displacement, an "absolute" response quantity, using only a few lower modes. The internal forces, that are computed from relative interstory displacements, were more sensitive to the truncation of higher modes. In inelastic analyses with elasto-perfectly plastic model, the maximum value of the story internal forces is approximately limited to the story yield forces. In this case, the ductility, defined as the ratio of the maximum story relative displacements to the static yield value, was found to be more sensitive to modal truncation than the internal forces. These conclusions were confirmed by Bathe and Gracewski (1981) that performed the same type of analyses on a similar building. Muscolino (1989) added pseudo-static correction to the PFM for the truncation of higher modes to study the elasto-plastic displacement response of simple 6 DOF structures subjected to harmonic loading. It was concluded that for structures subjected to low frequency content loading, the higher modes do not influence the elastic

response very much. However, the corresponding elasto-plastic response is influenced by the modal truncation, and the addition of a pseudo-static correction improved significantly the nonlinear response evaluated by the usual mode displacement method (MDM). Similar observations were made by Dungar (1982) that analyzed a 3 DOF elasto-plastic structure. Hanna (1989) combined the pseudo-force method with the mode-acceleration method to provide a static correction for the truncation of the higher modes in seismic analysis of moment-resisting frames. However, no systematic analyses to compare the quality of the modal solution with and without static corrections were reported. Chang and Mohraz (1990) studied the seismic displacement and internal force responses of a 6-story, rigid, and 19-story, flexible, shear buildings considering classical and non-classical damping. It was concluded that all modes should be considered for the 6-story structure, and that depending on the accuracy desired, fewer modes may be used for the flexible structure.

Gillies and Shepherd (1983) used the TSM to study the inelastic seismic response of a six-story planar moment-resisting frame subjected to the NS component of the 1940 El Centro Earthquake. Displacements and period elongations were reported. No systematic parametric evaluation of the effect of modal truncation was carried out. Idelsohn and Cardona (1985) studied the dynamic response of simple geometrically nonlinear structures subjected to harmonic loads by the TSM using truncated vector bases. In addition to the usual modal truncation error, a new source of error was identified each time a change of basis was performed. Incompatibility between the ability of the old basis and the new basis to represent the initial displacement, velocity and acceleration at the beginning of a new time-step introduced a continuously growing lack of equilibrium that produced an unstable solution. The proposed remedy to this problem was to improve the vector basis by the use of load-dependent Ritz vectors (Wilson et al. 1982, Léger and Wilson 1987) and by the addition of modal derivatives to avoid the need of updating the basis thus using a strategy similar to the PFM (Idelsohn and

Cardona 1985).

Review of past work concerning seismic energy dissipation and damping models for nonlinear seismic response analysis is presented in chapter 6 of this thesis.

1.3 SCOPE OF THE PRESENT STUDY

This research project is carried out in two phases. The first phase assesses different solution strategies to solve nonlinear seismic problems using vector superposition methods. The emphasis is put on the effect of modal truncation on the quality of the solution. The algorithms developed in the first phase are then used to study the effect of different mathematical representations of viscous damping on nonlinear response parameters.

In chapter 2, the general theory related to the solution of nonlinear systems in geometric coordinates is briefly presented. Two algorithms are then developed to extend the mode superposition method to nonlinear problems using either a tangent spectrum or a pseudo-force approach. A discussion about the selection of appropriate vector bases is also presented. A short description of the computer implementation of the two solution algorithms terminates this chapter.

Chapter 3 introduces various indicators to characterize the nonlinear solution carried out by a particular strategy. Importance is given to indicators that reflect the cumulative effects of nonlinear behaviour such as hysteretic and damping energy dissipation. The structures analyzed and the earthquake acceleration records used to conduct this study are presented in chapter 4. They are both adjusted to meet the requirements of the National Building Code of Canada (NBC 1990).

Numerical results concerning the solution strategies and the truncation of vector basis in nonlinear seismic analysis are given in chapter 5. Different proportional damping models suitable for earthquake response analysis are presented in chapter 6. A parametric study is performed to show the influence of these damping models on nonlinear response indicators in chapter 7. Finally, chapter 8 summarizes the work carried out and the main conclusions of this study.

CHAPTER 2

SOLUTION STRATEGIES FOR NONLINEAR DYNAMIC ANALYSIS

This chapter presents the strategies to solve the equation of motion of MDOF structures written as:

$$[M]\{\ddot{u}\} + [C]\{\dot{u}\} + [K]\{u\} = \{F(t)\} = \{f(s)\} \cdot g(t)$$
 (2-1)

where [M] is the mass matrix, [C] is the damping matrix, and [K] is the stiffness matrix. The vector {u} represents nodal displacements, and the dots indicate its derivatives. The load vector, {F(t)}, can be expressed as the product of a fixed spatial distribution, {f(s)}, and prescribed time function, g(t). The vector superposition method used in linear analysis is extended to nonlinear analysis using either pseudo-force or tangent spectrum approach.

2.1 SOURCES OF NONLINEARITIES

In a nonlinear problem, the matrices [M], [C], [K], and the vector {f(s)} of Eq. 2-1 can be a function of the displacements or its derivatives. The nonlinearities affecting those matrices and vector are from various sources. In structural angineering, the most frequent type of nonlinearity generally affects the stiffness matrix of the system. Figure 2.1 shows different sources of nonlinearity frequently observed in seismic response analysis of MDOF structures the P-Δ effects, the pounding with adjacent building, the uplift of one or more supports, and the nonlinear action-deformation of the resisting elements.

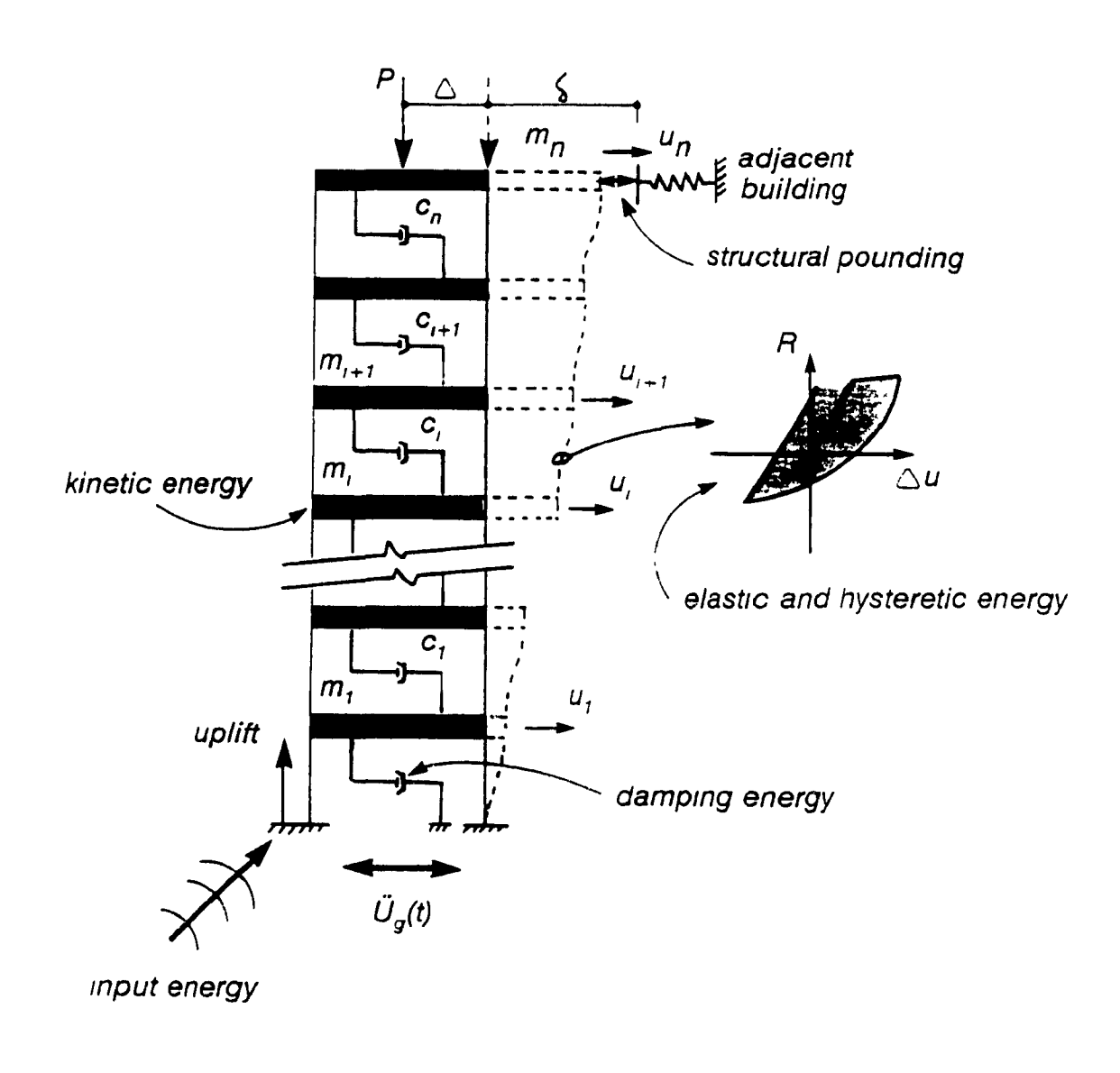


Figure 2.1. Sources of nonlinearities.

In this study, only material nonlinearities affecting the stiffness matrix will be considered. The damping matrix may therefore become nonlinear if it is taken as a combination of the tangent stiffness and mass matrices (Rayleigh damping described in chapter 6). Figure 2.2 shows a typical action-deformation of a bilinear hysteretic model of the structural element considered for numerical applications of the proposed solution strategies.

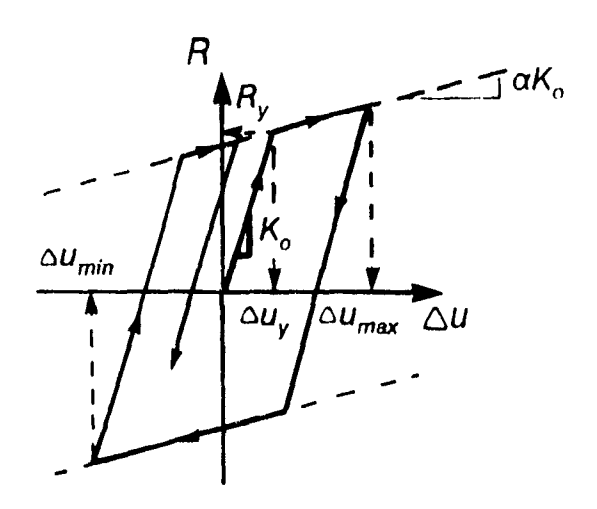


Figure 2.2. Action-deformation model of structural elements.

2.2 EQUATION OF DYNAMIC EQUILIBRIUM

The equation of dynamic equilibrium for seismic response analysis of a bilinear system in geometric coordinates is:

$$[M]\{\bar{u}\} + [C]_t\{\dot{u}\} + \{R(t)\} = -[M]\{r\}\bar{u}_g(t) = \{F(t)\}$$
 (2-2)

where [M] is the mass matrix, [C], is the tangent damping matrix, $\{R(t)\}$ is the nonlinear restoring force vector, $\{r\}$ is the influence vector from unit base displacement, and $u_g(t)$ is the specified ground acceleration. The restoring force vector, $\{R(t)\}$, can be written in terms of the tangent stiffness matrix, $[K]_t$, as:

$$\{R(t)\} = [K]_t[u] = ([K]_t + [K]_n)\{u\}$$
 (2-3)

where [K], is the linear stiffness corresponding to the reference state of the structure, and [K], is the stiffness component dependent on displacements. In nonlinear seismic analysis, viscous damping is generally modelled by a Rayleigh-type representation given as (Gillies and Shepherd 1983, Kanaan and Powell 1973):

$$[C]_{i} = a[M] + b[K]_{i} + b_{0}[K]_{i} = (a[M] + (b + b_{0})[K]_{i}) + b[K]_{n} = [C]_{i} + [C]_{n}$$
 (2-4)

Substituting Eqs 2-3 and 2-4 in Eq. 2-2 and then transferring all the nonlinear terms to the right hand side of the equation, we obtain the pseudo-force formulation of the equation of equilibrium:

$$[M]\{\ddot{u}\} + [C]_{i}\{\dot{u}\} + [K]_{i}\{u\} = \{F(t)\} - [K]_{n}\{u\} - [C]_{n}\{\dot{u}\}$$
 (2-5)

This formulation is also used to treat problems with nonproportional damping, where [C], then represents the nonproportional portion of the damping matrix and [K], is taken as zero (Claret and Venâncio-Filho 1991; Udwadia and Esfandian 1990; Ibrahimbegovic and Wilson 1989).

It is also possible in Eq. 2-2 to treat directly the nonlinearities of the system in the left hand side of the equation. This method is known as Newton-Raphson or tangent method. This procedure provides a fast rate of convergence since the tangent properties of the system are frequently updated to reflect the evolution of nonlinear behaviour. The method has the drawback that a reformulation of the system matrices is needed at each update. Therefore, the gain made with a fast convergence can be lost if frequent reformulations are required. Equation 2-5 takes all the nonlinear terms to the right hand side of the equation. This method is called the Modified Newton-Raphson or Pseudo-Force Method (PFM). It generally converges more slowly than the tangent method but does not require any reformulation of the system matrices. Figure 2.3 shows schematically the type of convergence achieved by both methods.

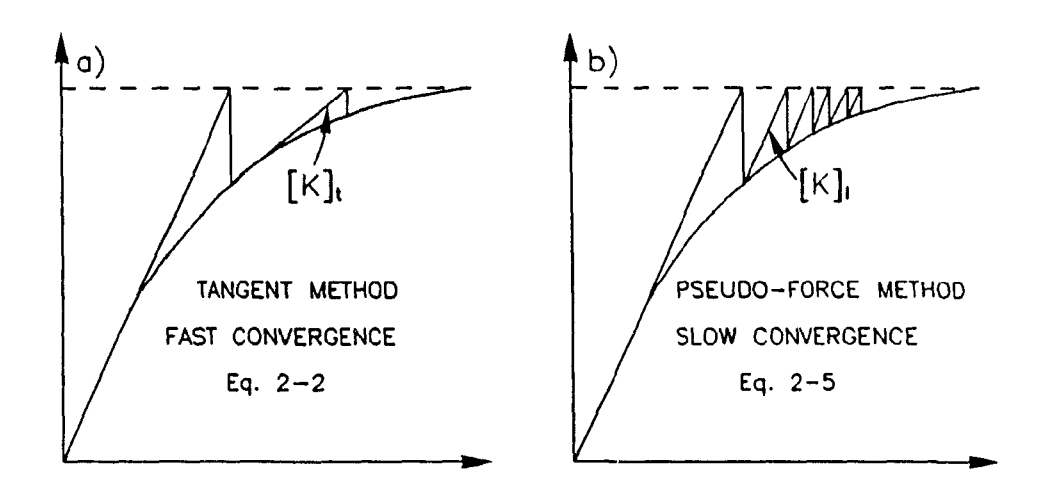


Figure 2.3. Rate of convergence of tangent and pseudo-force methods.

As shown in Figure 2.3, Eqs 2-2 and 2-5 have to be solved iteratively since the nonlinear portion of the matrices, [K]_n and [C]_n, are not known a priori. Step-by-step integration of the equations in their incremental forms is generally used in the solution. It is recognized that in geometric coordinates, Eq. 2-2 requires much less iteration than Eq. 2-5, but needs a reformulation of the matrices at each iteration (Bathe and Cimento 1980). The computer program DRAIN-2D (Kanaan and Powell 1973) uses a technique that does not involve iteration. It solves the equation of equilibrium using Eq. 2-2 and by applying the unbalanced load vector to the next time-step. The unbalanced load vector is simply a force vector representing the lack of equilibrium at each DOF. Therefore, the equilibrium is not achieved at every time-step and this procedure requires a small time-step to ensure a good quality of the solution.

2.3 VECTOR SUPERPOSITION IN NONLINEAR DYNAMIC ANALYSIS

2.3.1 Pseudo-Force Method (PFM).

The vector of nodal displacements, {u}, can be approximated by a linear combination of a set of linearly independent free-vibration elastic eigenvectors or [M]-orthonormal, [K], orthogonal, load dependent transformation vectors, [X], as:

$$\{u\} = [X]\{Y\}$$
 (2-6)

where {Y} is the generalized coordinates obtained by solving a system of equation written as:

$$[M]^*\{\ddot{Y}(t)\} + [C]^*\{\dot{Y}(t)\} + [K]^*\{Y(t)\} = \{F(t)\}^* - \{F(t)\}^*_0$$
 (2-7)

where $\{F(t)\}_{n}$ is defined as:

$$\{F(t)\}_{n}^{*} = [X]^{T}[K]_{n}[X]\{Y(t)\} + [X]^{T}[C]_{n}[X]\{\dot{Y}(t)\}$$
 (2-8)

and:

$$[M]^* = [X]^T [M][X] = [I]$$

$$[C]^* = [X]^T [C]_i [X] = [2 \cdot \xi \cdot \omega]$$

$$[K]^* = [X]^T [K]_i [X] = [\omega^2]$$

$$\{F(t)\}^* = [X]^T \{F(t)\}$$
(2-9)

In this study, the solution of Eq. 2-7 is carried out iteratively, as shown in Table 2.1, using Newmark-Beta average acceleration method. The nonlinear term, $\{F(t)\}_n$ is evaluated by computing the geometric displacements and velocities only at the DOF where nonlinear behaviour or added damping occur. In a large structural system with localized nonlinearities described by few DOF, this strategy will result in substantial computational saving as compared to the direct integration of the original equation of dynamic equilibrium. Moreover, the time-step required by vector superposition will generally be greater than that required by the step-by-step method of the original system of equations.

A- INITIAL CALCULATIONS:

- 1. Compute transformation $[K],[X] = [\omega^2][M][X]$ for eigenvectors vectors: Table 2.3 for LD vectors
- 2-Compute damping coefficients a and b_0 and form damping matrices $[C]_n = a\{M\} + b_0\{K\}_n$; $[C]_n$ matrices $[C]_n$; $[C]_n$:
- 3- Reduce the system of $[K]_i^* = [X]^T [K]_i [X]$ $[C]_i^* = [X]^T [C]_i [X]$ equation: $[M]^* = [X]^T [M][X] = [I]$
- 4- Form effective stiffness: $[\tilde{K}]^{\bullet} = [K]_{i}^{\bullet} + \frac{4}{\Delta t^{2}} [M]^{\bullet} + \frac{2}{\Delta t} [C]_{i}^{\bullet}$

B- FOR EACH TIME-STEP:

- 1- Form effective load vector: $\{\vec{F}(t)\} = \{\Delta F(t)\} + [M] \left(\frac{4}{\Delta t} \{\dot{u}(t)\} + 2\{\ddot{u}(t)\}\right) + 2[C], \{\dot{u}(t)\}$ initialize i=1, $\{\Delta u_0\} = \{0\}$ where $\{\Delta F(t)\} = \{F(t + \Delta t)\} \{F(t)\}$
- 2- Reduce load vector: $\{\tilde{F}(t)\}^{\bullet} = [X]^{T}\{\tilde{F}(t)\}$
- 3- Solve for incremental $[\tilde{K}]^*\{\Delta Y_i\} = \{\tilde{F}(t)\}^*$ displacements: $\{\Delta u_i\} = [X]\{\Delta Y_i\}$
- 4- Accumulate incremental $\{\Delta u_i(t)\} = \{\Delta u_{i-1}(t)\} + \{\Delta u_i\}$ displacements:
- 5- Compute incremental velocities and accelerations: $\{\Delta \dot{u}(t)\} = \frac{2}{\Delta t} \{\Delta u_i(t)\} 2\{\dot{u}(t)\}$ $\{\Delta \ddot{u}(t)\} = \frac{4}{\Delta t^2} \{\Delta u_i(t)\} \frac{4}{\Delta t} \{\dot{u}(t)\} 2\{\ddot{u}(t)\}$
- 7- State determination: $R(t+\Delta t) = ([K]_t + [K]_n) \{u(t+\Delta t)\}$
- 8- Equilibrium check: $\{RES\} = \{F(t+\Delta t)\} \{R(t+\Delta t)\} \{M\}\{\ddot{u}(t+\Delta t)\} \{M\}\{\ddot{u}(t+\Delta t)\} \{M\}\{\ddot{u}(t+\Delta t)\}$ $|F|\{RES\}|_2 > TOL \quad |i=i+1 \quad GOTO \quad 2 \quad \text{with} \quad \{\ddot{F}(t)\} = \{RES\}$ $\leq TOL \quad CONTINUE$
- 9- Proceed to next time-step.

2.3.2 Tangent Spectrum Method (TSM).

In the Tangent Spectrum Method, the transformation vectors are updated at each timestep when nonlinear behaviour is detected in the solution. The equilibrium equation in generalized coordinates using [M]-orthonormal tangent vectors, [X], can be written as:

$$[X]_{t}^{T}[M][X]_{t}(\ddot{Y}(t)) + [X]_{t}^{T}[C]_{t}[X]_{t}(\dot{Y}(t)) + [X]_{t}^{T}[K]_{t}[X]_{t}(Y(t)) = [X]_{t}^{T}\{F(t)\}$$

$$\{\ddot{Y}(t)\} + [C]_{t}^{T}\{\dot{Y}(t)\} + [K]_{t}^{T}\{Y(t)\} = \{F(t)\}^{*}$$
(2-10)

The tangerit solution strategy developed in this study is summarized in Table 2.2. Equilibrium iterations can be optionally performed in the system of equation expressed in generalized coordinates. The equilibrium unbalance can be compensated by computing the acceleration vector from the condition of dynamic equilibrium expressed in geometric coordinates as described in step B-10 in Table 2.2. This strategy provides a stable tangent solution, however the acceleration and velocity may trien differ significantly from the exact solution using a complete vector basis. From preliminary analyses, it has been found that a single update by time-step can result in a good approximation of the exact response. It has also been observed that the TSM is much more accurate when the update is performed at the second iteration as compared to a strategy that performs an update at the first iteration when nonlinear behaviour has been detected.

2.4 SELECTION OF VECTOR BASIS

The elastic, [X], or tangent, [X], transformation vectors can be computed from the $n \times n$ undamped free-vibration eigenproblems:

$$[K]_t[X] = [\omega^2][M][X]$$
 or $[K]_t[X]_t = [\omega^2]_t[M][X]_t$ (2-17)

When the vector basis, taken as eigenvectors, is truncated to r vectors (with r << n), it has

been shown that a better response is obtained for the PFM if a static correction is considered to compensate for the flexibility of the higher modes ignored in the superposition (Hanna 1989, Muscolino 1989). This static correction can be taken into account as (Léger and Wilson 1988)

$$\{u(t)\} = \sum_{i=1}^{r} \{X_i\} Y_i(t) + ([K]^{-1} - [X_r][\omega_r^2]^{-1} [X_r]^T) \{F(t)\}$$
 (2-12)

or
$$\{u(t)\} = \sum_{i=1}^{r} \{X_i\} Y_i(t) + [K]^{-1} (\{F(t)\} - \sum_{i=1}^{r} (\{X_i\}^T \{F(t)\}) [M] \{X_i\})$$
 (2-13)

where {X_i} is the eigenvector corresponding to the ith frequency. In Eqs 2-12 and 2-13, the first term corresponds to the modal superposition of generalized coordinates {Y_i}, with i ranging from 1 to r. The second term is a full static solution from which the contribution of modes 1 to r is removed. Léger and Wilson (1988) have demonstrated that using either Eq. 2-12 or 2-13 to take into account a static correction in mode superposition is equivalent.

Alternatively, load dependent transformation vectors generated by an inverse iteration type of scheme from the fixed spatial distribution of the seismic load can be used for [X] or [X], The algorithm to generate the load dependent vectors is shown in Table 2.3 (Léger and Wilson 1987). These vectors will include directly in the basis the static correction for the truncation of higher modes in superposition, and can be generated at a fraction of the computational cost required to obtain exact eigenvectors. For linear earthquake response analyses based on vector superposition methods, an effective mass corresponding to the part of the total mass responding to the earthquake in each vector, is commonly used as an indicator of the relative contribution of a particular vector to the global structural response. The cumulative effective "modal" mass, for a truncated set of r [M]-orthonormal eigen or load-dependent vectors is:

$$\theta_r = \frac{\sum_{l=1}^r p_l^2}{\{r\}^T [M] \{r\}} \cdot 100\% \tag{2-14}$$

where:

$$\rho_{I} = \{X_{I}\}^{T}[M]\{r\} \tag{2-15}$$

The value of e, can be monitored directly during the vector computation process. An appropriate

value, corresponding to 90% to 95% of the total mass, can be used to define a cutoff criterion in order to stop generating new vectors when a good representation of the spatial distribution of the earthquake load has been achieved.

Table 2.2. Tangent Spectrum Method (TSM).

A- INITIAL CALCULATIONS:

Perform operations described in block C-TANGENT PROPERTIES.

B-FOR EACH TIME-STEP:

1- Form effective load vector: $\{\vec{F}(t)\} = \{\Delta F(t)\} + [M] \left(\frac{4}{\Delta t} \{\dot{u}(t)\} + 2\{\ddot{u}(t)\}\right) + 2[C]_t \{\dot{u}(t)\}$ where $\{\Delta F(t)\} = \{F(t+\Delta t)\} - \{F(t)\}$

2- If i=2 and a change of basis is required, perform block C- TANGENT PROPERTIES

- 3- Reduce load vector: $\{\vec{F}(t)\}^* = [X]_t^T \{\vec{F}(t)\}$
- 4- Solve for incremental $[K]_t^* \{ \Delta Y_t \} = \{ F(t) \}^*$ displacements: $\{ \Delta u_t \} = [X]_t \{ \Delta Y_t \}$
- 5- Accumulate incremental $\{\Delta u_i(t)\} = \{\Delta u_{i-1}(t)\} + \{\Delta u_i\}$ displacements:

- 8- State determination: $R(t+\Delta t) = [K]_t \{u(t+\Delta t)\}$

If i=1 and a member changes state, an update of the basis is required.

- 10- reestablish equilibrium: $\{\ddot{u}(t+\Delta t)\} = [M]^{-1}(\{F(t+\Delta t)\} \{R(t+\Delta t)\} [C]_t\{\dot{u}(t+\Delta t)\})$
- 11- Proceed to next time-step.

Table 2.2. Tangent Spectrum Method (continued).

C-TANGENT PROPERTIES:

- 1- Compute tangent vector $[K]_t[X]_t = [\omega^2]_t[M][X]_t$ for eigenvectors shapes: Table 2.3 for LD vectors
- 2- Compute damping matrix: $[C]_t = a_t[M] + b_t[K]_t + b_0[K]_t$ (if required)
- 3- Reduce the system of $[K]_t^* = [X]_t^T [K]_t [X]_t$ $[C]_t^* = [X]_t^T [C]_t [X]_t$ equation: $[M]^* = [X]_t^T [M][X]_t = [I]$
- 4- Form effective stiffness: $[\bar{K}]_t^* = [K]_t^* + \frac{4}{\Delta t^2} [M]^* + \frac{2}{\Delta t} [C]_t^*$

Table 2.3. Load dependent vectors (LD).

- 1- Dynamic equilibrium equation: $[M]\{\ddot{u}\} + [C]\{\dot{u}\} + [K]\{u\} = \{f(s)\} g(t)$
- 2- Triangularize stiffness matrix: $[K] = [L]^{T}[D][L]$
- 3- Solve for initial static deflected shape, $\{U_0\}$: $[K]\{U_0\} = \{f(s)\}$
- 4- Solve for Ritz vectors i=1,...,r-1: $[K]\{\overline{X}_i\} = [M]\{U_{\underline{i-1}}\}$ $c_i = \{X_i\}^T [M]\{X_i\}$
 - [M]-orthogonalization $\{\bar{X}_i\} = \{\bar{X}_i\} \sum_{j=1}^{i-1} c_j \cdot \{X_j\}$ (skip for i=1) $v = (\{\bar{X}_i\}^T [M] \{\bar{X}_i\})^{1/2}$ [M]-normalization $\{X_i\} = \{\bar{X}_i\} \cdot 1/v$ update static vector $c_{ul} = \{U_{l-1}\}^T [M] \{X_l\}$ $\{U_i\} = \{U_{l-1}\} c_{ul} \cdot \{X_l\}$
- 5- Add static residual, $\{U_{r-1}\}_{r=1}^{T}$, as static correction $\{X_r\}_{r=1}^{T}$ $\{U_{r-1}\}_{r=1}^{T}$ $\{U_{r-1}\}_{r=1}^{T}$ $\{U_{r-1}\}_{r=1}^{T}$ $\{U_{r-1}\}_{r=1}^{T}$

2.5 COMPUTER IMPLEMENTATION OF NONLINEAR SOLUTION ALGORITHMS

A FORTRAN computer program has been developed to integrate the solution algorithms presented in Tables 2.1, 2.2 and 2.3. The program is also capable of carrying the solution in geometric coordinates if the transformation to a reduced system of equations is ignored. Many computational variants are possible depending if the coordinate transformation decouples the reduced system or not. This is a function of the type of damping model retained, and also of the [K]-orthogonality of the [M]-orthonormal vector basis that is not a mandatory requirement for the validity of the proposed solution strategies. The program has been developed using the Newmark-Beta method to solve either coupled or uncoupled reduced systems, and maintain a high degree of compatibility between the PFM, TSM, and the solution in geometric coordinates. Extensive post-processing options have been provided to tabulate and interpret the various nonlinear response indicators considered in the study.

CHAPTER 3

INDICATORS TO CHARACTERIZE NONLINEAR BEHAVIOUR

This chapter presents the indicators used to monitor the structural response obtained from various algorithms to solve nonlinear seismic problems. These indicators can be classified into two categories. The first category relates to the time-histories of response parameters such as displacements, internal forces, ductility, and periods of vibration. The intensities of the time-history responses are characterized by the maximum values of these parameters over the duration of the event. The second category relates to cumulative effects such as hysteretic energy dissipation, and total number of yield excursions. Both categories are required to quantify the level of anticipated seismic damage, and are used extensively in earthquake resistant design and analysis of structural systems.

3.1 EVOLUTION OF TANGENT MODAL PROPERTIES

One advantage of using tangent modes superposition in nonlinear dynamic analysis is the ability to follow the evolution of the modal properties. This provides a rationalization of the nonlinear behaviour of the seismic response in an elastic format. Moreover, it permits a better control on some parameters of the nonlinear solution such as the number of modes that should be retained in the superposition.

The evolution and maximum values of the periods of vibration in a seismic analysis can give a good indication of the severity of the nonlinear response of a structure during an earthquake. Furthermore, for elasto-plastic type of resisting elements, the periods of the structure will increase as the structure becomes nonlinear. Therefore it will generally attract less seismic

load. One can thus rationalize the importance of dynamic modification of the structural properties on the reduction of seismic load. Dipasquale (1989) proposed the following damage index based on the maximum fundamental period, $T_{1,max}$, reached by the nonlinear solution:

$$\delta = 1 - \frac{T_{1 \, elastic}}{T_{1 \, max}} \tag{3-1}$$

where δ represents a global damage index that reflects the importance of the softening effect produced by plastic deformations.

3.2 DISPLACEMENT DUCTILITY

The displacement ductility demand of a member with hysteretic behaviour is used as an indicator of the severity of the nonlinear response. Many modern codes uses the ductility concept in reducing the seismic design force to account for the ability of the structures to deform inelastically. The displacement ductility is defined as the ratio of the member relative displacement during a yield excursion normalized by the yield static displacement, ΔU_y , as shown in Figure 2.2. Only the maximum absolute value of the ductility demand of each member will be retained in the nonlinear analyses.

3.3 ENERGY INDICATORS

Energy balance considerations are used extensively to characterize the behaviour of a structure that experiences nonlinearities during an earthquake (Uang and Bertero 1990; Conte et al. 1990; Hadidi-Tamjed 1988). The energy reflects the interaction of the displacements and related forces since it is the product of those two parameters.

3.3.1 Energy balance

The energy calculations are performed using the "absolute" energy equation, (Uang and Bertero 1990). The dynamic equation of equilibrium in its absolute form is writen as:

$$[M]\{\ddot{u}_t\} + [C]\{\dot{u}\} + \{R(t)\} = 0 \tag{3-2}$$

where [M] is the mass matrix, [C] is the damping matrix, $\{R(t)\}$ is the vector of nonlinear restoring force, and u_t is the absolute structural displacement given by the sum of the relative displacement, u_t , and the ground displacement u_g . Integrating Eq. 3-2 with respect to the displacement, we get the following energy balance expression:

$$\int ([M]\{\bar{u}_t\})^T \{du\} + \int ([C]\{\dot{u}\})^T \{du\} + \int \{R(t)\}^T \{du\} = 0$$
 (3-3)

replacing $\{u\}$ by $(\{u_i\} - \{u_a\})$ in the first term of Eq. 3-3:

$$\int ([M]\{\bar{u}_t\})^T \{du\} = \int ([M]\{\bar{u}_t\})^T (\{du_t\} - \{du_g\}) = \int ([M]\frac{d}{dt}\{\dot{u}_t\})^T \{du_t\} - \int ([M]\{\bar{u}_t\})^T \{du_g\} \\
= \frac{\{\dot{u}_t\}^T [M]\{\dot{u}_t\}}{2} - \int ([M]\{\ddot{u}_t\})^T \{du_g\} \tag{3-4}$$

substituting the result of Eq. 3-4 in Eq. 3-3:

$$\frac{\{\dot{u}_t\}^T[M]\{\dot{u}_t\}}{2} + \int ([C]\{\dot{u}\})^T\{du\} + \int \{R(t)\}^T\{du\} = \int ([M]\{\ddot{u}_t\})^T\{du_g\}$$
 (3-5)

In Eq. 3-5, the kinetic energy is:

$$E_{K}(t) = \frac{\{\dot{u}_{t}\}^{T}[M]\{\dot{u}_{t}\}}{2}$$
 (3-6)

using $\{du\} = \{\dot{u}\}dt$, the damping energy becomes:

$$E_{D}(t) = \int ([C]\{\dot{u}\})^{T} \{du\} = \int_{0}^{t} \{\dot{u}\}^{T} [C]\{\dot{u}\} dt$$
 (3-7)

and the input energy becomes:

$$E_{t}(t) = \int ([M]\{\bar{u}_{t}\})^{T} \{du_{g}\} = \int_{0}^{t} \{\dot{u}_{g}\}^{T} [M]\{\bar{u}_{t}\} dt$$
 (3-8)

It should be noted that using the absolute energy equation yields expressions for the input energy, E_{ii} , and kinetic energy, E_{ki} , that include the effects of rigid body translation of the structure. Finally the resisting force, $R_{i}(t)$ of each element i is composed of recoverable strain energy, E_{Si} , and dissipated or irrecoverable hysteretic energy, E_{Hi} . Referring to Figure 2.2, the strain energy, E_{S} for the total number of elements, nel, is:

$$E_{S}(t) = \sum_{i=1}^{nel} E_{Si}(t) = \sum_{i=1}^{nel} \frac{R_{i}(t)}{2K_{0i}}$$
 (3-9)

and E_H is computed as follows:

$$E_{H}(t) = E_{H}(t-\Delta t) + \sum_{i=1}^{not} \frac{2R_{i}(t-\Delta t) + [\Delta u_{i}(t) - \Delta u_{i}(t-\Delta t)] \cdot K_{ti}}{2} \cdot [\Delta u_{i}(t) - \Delta u_{i}(t-\Delta t)] + \frac{R_{i}(t-\Delta t) \cdot \Delta u_{i}(t-\Delta t)}{2} - \frac{R_{i}(t) \cdot \Delta u_{i}(t)}{2}$$
(3-10)

where $\mathrm{K}_{\!\scriptscriptstyle H}$ is the current stiffness of element i. Finally Eq. 3-3 yields to:

$$E_{i}(t) = E_{K}(t) + E_{D}(t) + E_{S}(t) + E_{H}(t)$$
 (3-11)

with all terms described in Eqs 3-6 to 3-10. It should be noted, regarding Eqs 3-6 to 3-10, that the kinetic energy and recoverable strain energy are instantaneous quantities, while input energy, the damping energy, and the hysteretic energy are cumulative quantities.

Since all energy terms are computed individually, the error in energy balance can be used as a global indicator of the equilibrium acheived by a solution strategy. The normalized error in energy balance, EEB(t), can be defined as:

$$EEB(t) = \frac{|E_{i}(t) - E_{K}(t) - E_{D}(t) - E_{H}(t) - E_{S}(t)|}{|E_{i}(t)|}$$
(3-12)

The value of EEB(t) should be very small to ensure the reliability of seismic response indicators produced by a specific strategy.

3.3.2 Energy dissipation

The ratio of hysteretic energy to the amount of input energy, E_H/E_H is computed for each analysis at the end of the earthquake record. For inelastic systems, the values of the kinetic and strain energies are generally small as compared to the damping and hysteretic energies at the end of the earthquake. The total input energy at the end of the ground motion, E_H is therefore approximately equal to the total dissipated energy, TDE, given by the sum of E_H and E_D . Thus, the ratio E_H/E_H can be also interpreted as the ratio E_H/TDE indicating the relative importance of the hysteresis response mechanism on the total energy dissipated.

3.3.3 Rate of energy dissipation, power

Various indicators related to the rate of energy (power) responses are also computed. These quantities indicate how fast the energy is imparted and dissipated by the structure. It has been postulated by Conte et al. (1990) that a low and uniform, or a highly variable, spiky, rate of hysteretic energy dissipation must respectively correspond to different levels and types of damage. Much research works remain to be done in this area, it is therefore important at this stage to study the influence of the mathematical model adopted for the viscous damping on the power response. The power indicators are adapted from Conte et al. (1990). They are defined as the maximum positive rate of normalized earthquake input energy, P_{ii}, the maximum rate of normalized hysteretic energy dissipated, P_H, and the maximum rate of normalized viscous damping energy, P_D, given as:

$$P_{I} = MAX \left[\frac{dE_{I}(t)}{dt} \cdot \frac{1}{\left\{ \Delta U_{y} \right\}^{T} \cdot \left\{ R_{y} \right\}} \right]$$
 (3-13)

$$P_{H} = MAX \left[\frac{dE_{H}(t)}{dt} \cdot \frac{1}{\left\{ \Delta U_{y} \right\}^{T} \cdot \left\{ R_{y} \right\}} \right]$$
 (3-14)

$$P_D = MAX \left[\frac{dE_D(t)}{dt} \cdot \frac{1}{\{\Delta U_y\}^T \cdot \{R_y\}} \right]$$
 (3-15)

where $\{R_y\}$ is the vector of yield force of the members equal to the seismic lateral design forces of the multistory buildings for a force reduction factor R=1, and $\{\Delta U_y\}$ is the corresponding yield displacements as shown in Figure 2.2.

3.4 YIELDING SEQUENCE

The yielding sequence plays a very important role in evaluating the potential damage of a structure due to cumulative effects such as low cycle fatigue. The number of times that a member yields combined with the ductility demand provide indications about the type of damage that can occur. A large number of yield excursions combined with low ductility demand is likely to produce fatigue type of damage. On the other hand, few yield excursions with a high ductility demand will produce damage by lost of capacity. In this study, the number of yield excursions and the ductility demand are analysed as separate parameters. Some relatively complex indicators have been developed to link these two parameters (Hadidi-Tamjed 1988).

CHAPTER 4

SYSTEMS ANALYSED

This chapter presents the MDOF structural systems developed to perform numerical applications. The structures are designed according to National Building Code of Canada 1990 (NBC 1990). The seismic loads consist of three well known earthquake acceleration records that have been grouped around the NBC 1990 elastic design spectra by a proper scaling method.

4.1 STRUCTURAL MODELS

The multistory buildings are represented by typical MDOF "shear beam" structures as shown in Figure 2.1. In this model, the number of DOF corresponds to the number of stories. Seven buildings with 1, 3, 5, 10, 15, 20 and 25 DOF are considered for numerical applications

4.1.1 Element action-deformation model

The type of structural element action-deformation model used in the analyses is a bilinear hysteretic model as shown in Figure 2.2. Since only material nonlinearities are considered, the bilinear hysteretic model simulates the interstory resisting force of the members. This type of element has the ability to store strain energy and to dissipate energy trough hysteretic behaviour. The hysteretic energy dissipated by this type of element is computed from Eq. 3-10 and is represented schematically by the area enclosed by the solid curve on Figure 2.2.

4.1.2 Design procedure

Seismic provisions of the National Building Code of Canada (NBC 1990) are used to design the structures. In NBC, the total minimum lateral seismic force, that is used with a load

factor equal to 1, is given by V = (Ve / R) U where Ve is the equivalent lateral force at the base of the structure representing the elastic response. The base shear is distributed over the height of the structure by an inverted triangular distribution plus an additional force at the top as shown in Figure 4.1. The parameter R is the force modification factor to account for nonlinear ductile behaviour, and U is a calibration factor representing the desired level of protection based on experience. The value of R ranges from 1, for non-ductile structural systems expected to remain elastic under the design earthquake ground motion, to 4 for ductile moment resisting frames with good seismic detailing. For SDOF structures, the value of R is directly related to the displacement ductility demand of the systems. The total force reduction from the elastic level can be interpreted as the product of a global ductility factor equal to R, and an overstrength factor equal to 1/U.

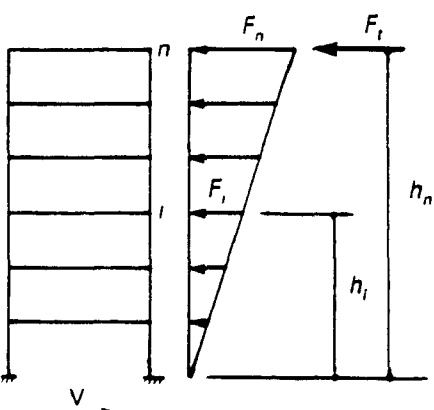


Figure 4.1. NBC pseudo-static earthquake loading distribution.

The structures are assumed to be located in Victoria, B.C. considering a peak ground velocity (PGV) of 0.26 m/s and a peak ground acceleration (PGA) of 0.26 g. The structures analyzed are designed for an actual base shear equal to V/U to consider the effect of overstrength on the nonlinear response (Uang 1991). A nondimensional parameter, η , can be used to characterize the strength of each structure. The parameter η is expressed as the ratio of the design base shear at yield, V/U, to the maximum effective force applied during the earthquake:

$$\eta = \frac{V}{[(M \cdot \bar{u}_{\text{gmax}}) \cdot U]} \tag{4-1}$$

where M is the total mass of the system and \ddot{u}_{gmax} is the PGA expressed in consistent units with the mass.

The design procedure can be summarized as follows:

- 1. Assume a uniform "unit" mass of 100 kN-sec²/m at each floor.
- Compute the total minimum lateral seismic force at the base of the structure considering overstrength V/U. The fundamental period of vibration is assumed equal to 0.1N as specified by the code.
- 3. Compute the lateral distribution of the seismic load V/U over the height of the structure according to NBC.
- 4. Take the yield forces equal to the story shears.
- 5. Assume a linear variation of the stiffness over the height of the structure.
- 6. Adjust the top and bottom stiffness to give almost equal inter-story drifts at the top and bottom of the building when loaded by the NBC pseudo-static load (Figure 4.1)
- 7. Scale all stiffness coefficients to obtain a fundamental period of vibration equal to 0.1N where N is the number of stories.
- 8. The properties of the strongest member are taken for grouped members. For structures with a large number of stories, keep the properties unchanged for two or three stories.
- 9. Verify that the interstory drift limitation specified by the code is met.

4.1.3 Structural properties

The procedure outlined in the previous section is applied to the 1, 3, 5, 10, 15, 20 and 25 DOF structures to define the properties of the members. Table 4.1 lists the initial stiffness and the yield force of each member or group of members for all structures. The yield forces in this table correspond to a force modification factor, R=4. Those values should be multiplied by 4 to obtain R_y for R=1, by 2 to obtain R_y for R=2, and so on. Since the method used to scale the earthquakes does not give uniform PGA for the three earthquakes, the strength parameter, η , is varying from an earthquake to another. The values of η are listed in Table 4.2.

able 4.1.	Proper	ties of struc	tures analyzed.				
No of stories	Level ¹	K₀ (kN/m)	Ry² (kN)	No. of stories	Level ¹	K₀ (kN/m)	R _y ² (kN)
1	1	395000	191	20	1-2	231000	1352
			}		3-4	211750	1336
3	1	274000	540		5-6	192500	1293
	2	205000	450		7-8	173250	1236
	3	137000	270		9-10	154000	1153
					11-12	134750	1048
5	1	245700	676		13-14	115500	920
	2	210600	631		15-16	96250	771
	3	175500	541		17-18	77000	599
	4	140400	406		19-20	57750	405
	5	105300	225				
10	1-2	248000	957	25	1	232000	1513
	3-4	201500	908		2-4	220400	1509
	5-6	155000	795		5-7	197200	1474
	7-8	108500	617		8-10	174000	1405
	9-10	62000	374		11-13	150800	1301
					14-16	127600	1163
15	1	252000	1172		17-19	104400	991
	2-3	224000	1163		20-22	81200	783
	4-5	196000	1119		23-25	58000	541
	6-7	168000	1041				
	8-9	140000	927				
	10-11	112000	779				
	12-13	84000	595				
	14-15	56000	377				

Strength parameter, η , of structures analyzed for R=4. **Table 4.2.**

Earthquakes				
El Centro	Parkfield	Taft		
η	η	η		
0.59	0.72	0.51		
0.55	0.68	0.48		
0.42	0.51	0.36		
0.29	0.36	0.25		
0.24	0.30	0.21		
0.21	0.26	0.18		
0.19	0.23	0.16		
	η 0.59 0.55 0.42 0.29 0.24 0.21	El Centro η Parkfield η 0.59 0.72 0.55 0.68 0.42 0.51 0.29 0.36 0.24 0.30 0.21 0.26		

¹ Each level has a mass of 100 kN-sec²/m.
² R_y is given for R=4, 2R_y corresponds to R=2.

4.2 EARTHQUAKE LOADING

Three earthquakes have been selected to perform the numerical analyses. Since the structures are designed according to the NBC 1990, the earthquake records are scaled such that they fit as well as possible the elastic response spectra of the NBC 1990.

4.2.1 Selected earthquakes

The selected earthquake accelerograms represent different types of seismic loading. The SOOE component of the 1940 El Centro earthquake contains a broad range of frequency. The N65E component of the 1966 Parkfield earthquake is representative of a single pulse loading. Finally the S69E component of the 1952 Taft earthquake contains high frequency loading and strong shaking is of long duration. The first 20 seconds of all records are considered. The three unscaled earthquakes are shown in Figure 4.2.

4.2.2 Scaling method

The scaling method proposed by Schiff (1988) is used to group the elastic spectra of the earthquakes around the NBC elastic design spectra corresponding to a zonal velocity to acceleration ratio equal to unity and a PGV=0.26 m/s. The three earthquakes are first scaled such that they have the same spectral intensity, SI_v, in the velocity range. The spectral intensity is defined as the area under the curve of the elastic spectra normalized by the specified frequency range:

$$SI_{v} = \frac{1}{3.0 - 0.5} \int_{T - 0.5}^{T - 3.0} PS_{v}(T) \cdot dT$$
 (4-2)

where PS_v is the pseudo velocity for 5% damping, and T is the period in seconds. This gives a first scaling factor, F_1 , for each accelerogram that tends to group the records together in the medium and long period range. The three accelerograms are then scaled by a unique scaling factor, F_2 to position them around the NBC elastic spectra. The scaling factor, F_2 , is computed

by dividing the spectral intensity in the acceleration range, SI_{ai} of NBC by the average of SI_{a} for the three accelerograms already scaled by F_{i} , SI_{a} is given by:

$$SI_{e} = \frac{1}{0.5 - 0.25} \int_{T-0.25}^{T-0.5} PS_{e}(T) \cdot dT$$
 (4-3)

where PS_a is the pseudo absolute spectral acceleration for 5% damping.

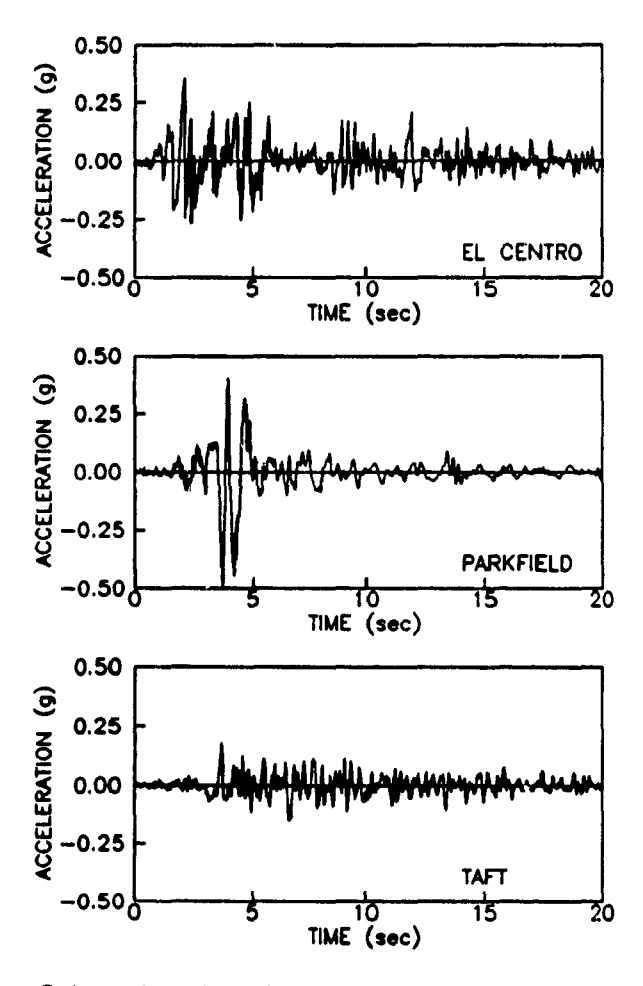


Figure 4.2. Selected earthquakes.

Table 4.3 gives the intensities and the scaling factors for all accelerograms. The last column of Table 4.3 gives the PGA of the scaled records. Figure 4.3 shows the spectra for the

three scaled accelerograms compared with the NBC spectra. Figure 4.3d shows the average and the envelope of the three scaled records compared with the NBC design spectra. It is observed that a very good agreement between the earthquake response spectra and the NBC design spectra is obtained from this scaling method even if there is some variations in the short period range (T < 0.5 sec).

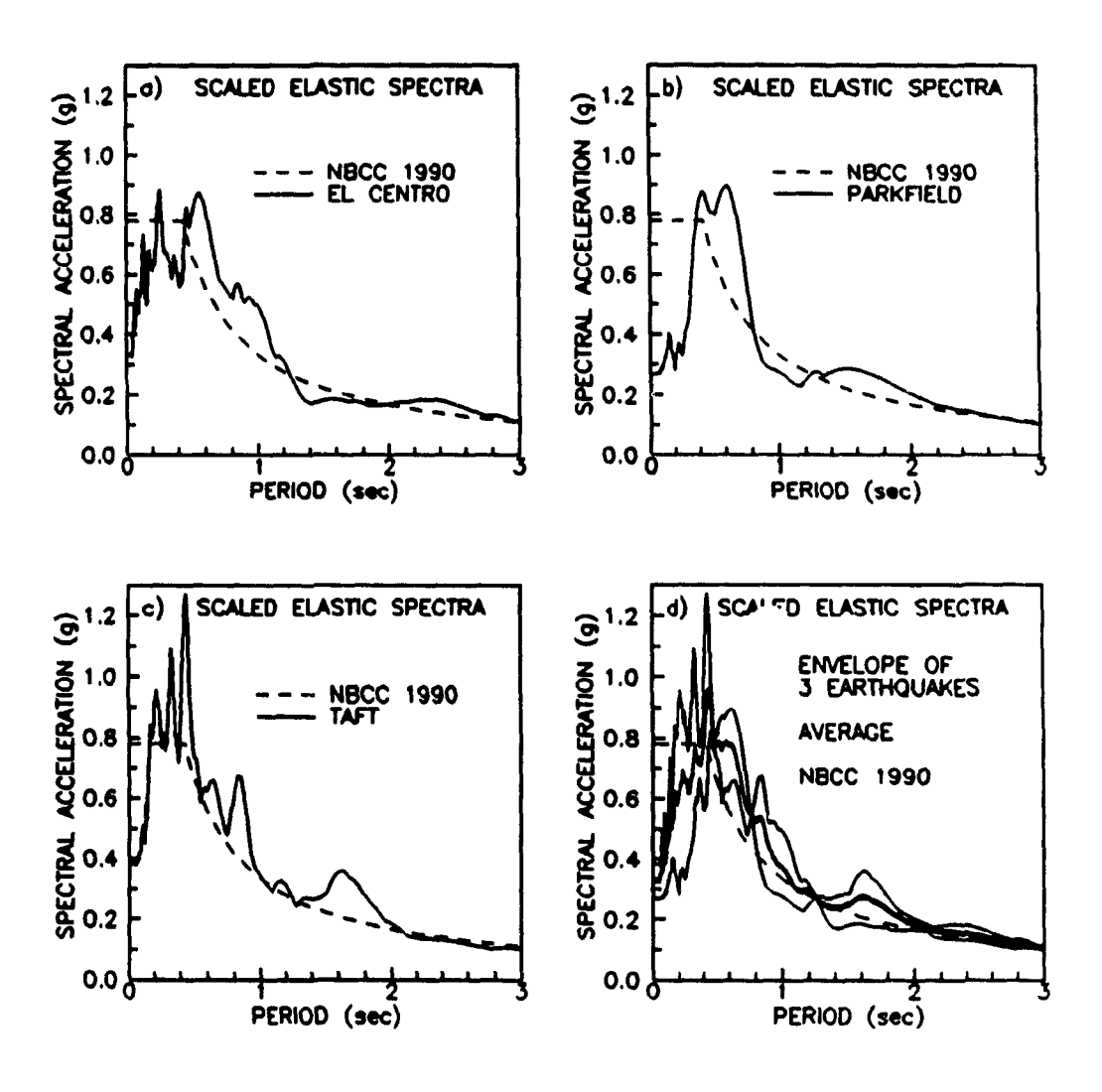


Figure 4.3. Scaled Earthquake spectra.

Table 4.3. Scaling factors for the earthquake records.

	SI _v	F,	SI.	F ₂	PGA (g)
El Centro	0.613	1.73	1.246		0.3316
Parkfield	1.059	1.00	1.216	0.55	0.2691
Taft	0.273	3.88	1.676		0.3829
NBC 1990			0.764	:	

CHAPTER 5

NONLINEAR SEISMIC RESPONSE USING VECTOR SUPERPOSITION

The performances of the algorithms based on the Pseudo-Force Method (PFM) and Tangent Spectrum Method (TSM) that have been developed in chapter 2 are investigated in this chapter. The main objective of this study is to assess the effects of the truncation of the vector basis on nonlinear response parameters described in chapter 3. The accuracy and the numerical stability of the algorithms are investigated.

The 5-story and 25-story buildings subjected to the scaled El Centro earthquake are used for the analyses. To maintain compatibility between the PFM and the TSM, the viscous damping is taken as Rayleigh type based on the initial elastic properties of the systems. The first mode and the mode at which 95% of effective modal mass is included in the solution are damped at 5% critical. The yield forces are those corresponding to a force reduction factor, R, equal to 4. A strain hardening ratio, α , of 10% is considered for all the members in both structures.

5.1 TANGENT SEISMIC RESPONSE ANALYSIS

The use of a tangent solution algorithm to perform a nonlinear analysis in generalized coordinates provides several advantages such as those described in the introduction of this thesis. The additional informations available from the tangent modal properties allow to develop

a better understanding of the nonlinear behaviour.

5.1.1 Evolution of tangent modal properties

Figure 5.1 shows the input accelerogram, and an example of the variation in the fundamental period of vibration, and the number of modes required to maintain 95% of effective modal mass in the solution using the TSM-MDM for the 25-story building. The instantaneous period of the first mode increases from 2.5 sec for elastic response to a maximum of approximately 6.8 sec when the system responded inelastically. For elastic response, modes 1 to 5 should be included to maintain 95% of effective modal mass while for inelastic response this range increases to modes 1 to 10.

5.1.2 Performance of tangent solution

Figure 5.2a illustrates the numerical stability of the TSM-MDM using Δt =0.01 sec with equilibrium iterations for the 25-story building. When a complete basis is used, the solution where { \ddot{u} } is computed from the integration operator is numerically stable. When a truncated set of vectors is used, instability soon appears after the first change of basis as shown by the top displacement response using 11 vectors. The addition of 6 vectors only delays the time at which the instability arises as shown by the response considering 17 vectors. This instability is due to the inability of the updated truncated vector basis to represent accurately the initial conditions computed from the previous time-step considering a different basis. It is possible to obtain a stable solution by computing { \ddot{u} } from the condition of equilibrium at the end of each time-step. However depending on the number of vectors considered, the accelerations, { \dot{u} } and the velocities, { \dot{u} }, might significantly deviate from the solution carried out with a complete basis. It should be noted that restoring equilibrium at the end of each time-step also provides some form of correction for the lack of equilibrium introduced by the truncation of higher modes.

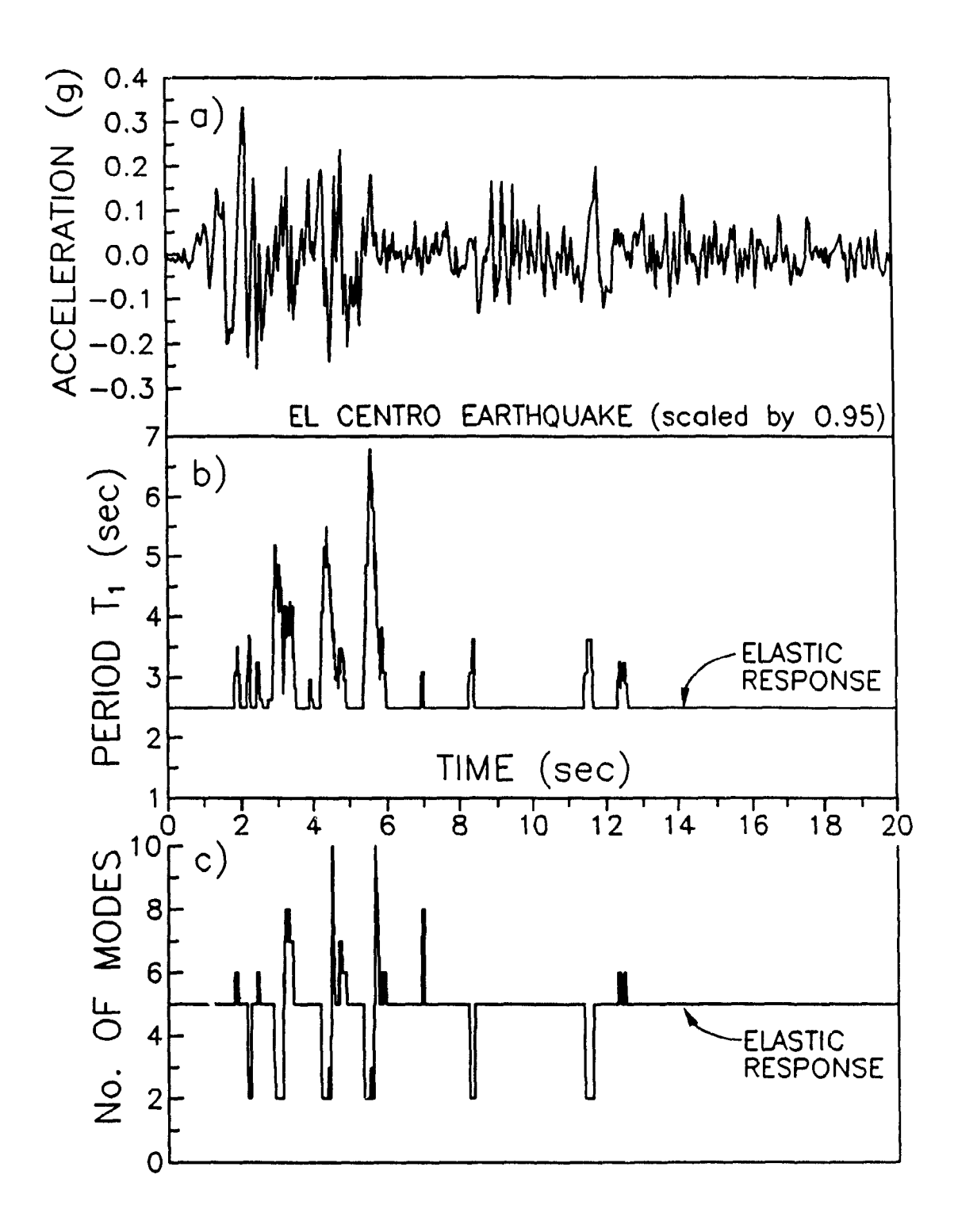


Figure 5.1. Input motion and evolution of tangent modal properties for 25-story building.

- (a) El Centro accelerogram.
- (b) Evolution of fundamental period, T₁.
- (c) No. of modes for 95% of effective modal mass.

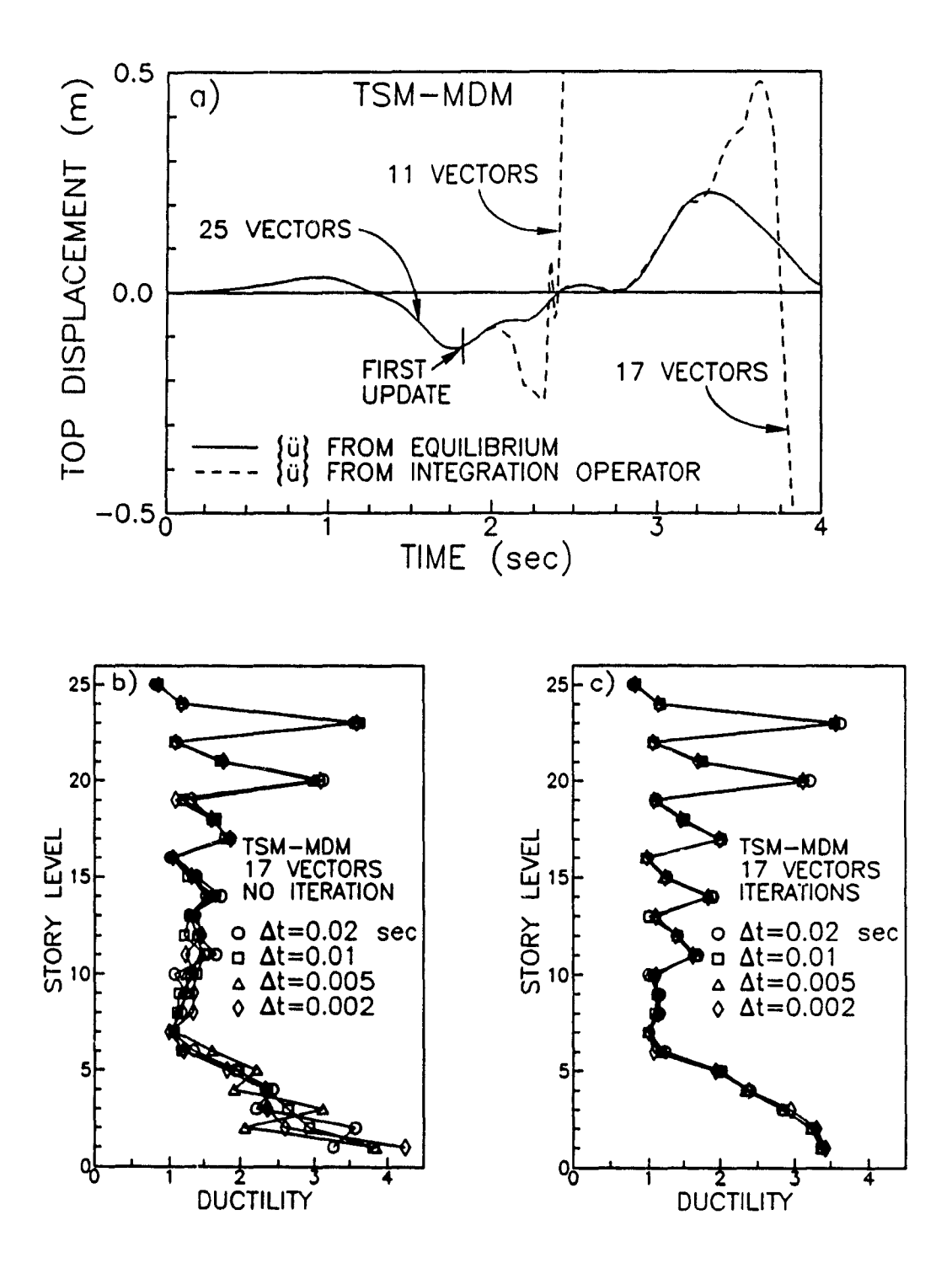


Figure 5.2. Performance of Tangent Spectrum Method for 25-story building.
(a) Effect of computing acceleration vector from the condition of dynamic equilibrium at time t + Δt.

- (b) Ductility demand for solution without equilibrium iteration.
- (c) Ductility demand for solution with equilibrium iterations.

Figures 5.2b and 5.2c show the effect of equilibrium iterations on the peak ductility demand considering the TSM-MDM strategy with different time-steps. The solution without iteration, as shown in Figure 5.2b, is sensitive to the selected time-step specially in the bottom stories. When equilibrium iterations are used, as shown in Figure 5.2c, the response is almost independent of the time-step. An accurate response is obtained using Δt as large as 0.02 sec corresponding to the time interval used to describe the input earthquake accelerations. The TSM with equilibrium iterations is therefore very advantageous to limit the number of basis update during the solution as shown in Table 5.1.

Table 5.1. Effects of equilibrium iterations and time-step on the number of basis updates.

Method	Time-step	Number of basis updates		
	∆t (sec)	with iterations	without iteration	
TSM-MDM	0.02	102	142	
	0.01	140	255	
1	0.005	164	500	
	0.002	201	927	
TSM-LDM	0.02	99	152	
	0.01	133	258	
1	0.005	164	500	
İ	0.002	216	1033	

The use of the TSM-LDM considering 17 vectors, required for energy convergence, decreases the CPU time by a factor of about two with respect to the TSM-MDM. The CPU time for the TSM-MDM is obtained by using the Lanczos method as the eigensolver. For a large structural system this difference would be much more significant, especially if the more robust subspace iteration algorithm is selected as the eigensolver. For this small system, no significant CPU time differences are observed between the PFM-MDM and the PFM-LDM since the vector basis is computed only once. The PFM solutions require approximately 15% and 30 % of the TSM-MDM and TSM-LDM execution time, respectively.

5.2 EFFECTS OF VECTOR BASIS TRUNCATION

5.2.1 Convergence of nonlinear response indicators - 25-story building

Figure 5.3a shows the time-history response of the top displacement using the TSM-LDM. A very good agreement is obtained for large-amplitude displacement oscillations considering only 5 vectors. For low-amplitude oscillations there is minor deviations from the "exact" response using 25 vectors that was found virtually identical with the solution in geometric coordinates. Figure 5.3b shows the force response in level 20. The 5-vector solution misses all the peak force responses. The 11-vector solution is almost identical with the "exact" force response. Further investigations have shown that for the systems analyzed, the ductility demand computed from truncated vector bases follows closely the convergence characteristics of the force response. Therefore, in subsequent comparative analyses, the emphasis is put on the ductility demand and the energy response.

Figure 5.4 describes the effect of the number of transformation vectors on the peak ductility demand for different solution strategies applied to the 25-story building. A time-step Δt = 0.01 sec and equilibrium iterations are used in all analyses. The results shown in Figure 5.4a and 5.4b indicate that the peak ductility response is quite sensitive to vector basis truncation when the PFM is used. The solutions computed using eigenvectors, PFM-MDM, and load-dependent vectors, PFM-LDM, yield comparable global performances. The truncated PFM-MDM ductility response is more accurate in the top stories while the PFM-LDM response is more accurate in the bottom stories. Figures 5.4c and 5.4d indicate that the peak ductility responses based on the TSM is much less sensitive to basis truncation than the solutions obtained from the PFM. Excluding the solutions carried out with 5 vectors, it is shown that the MDM and the LDM yield almost identical results.

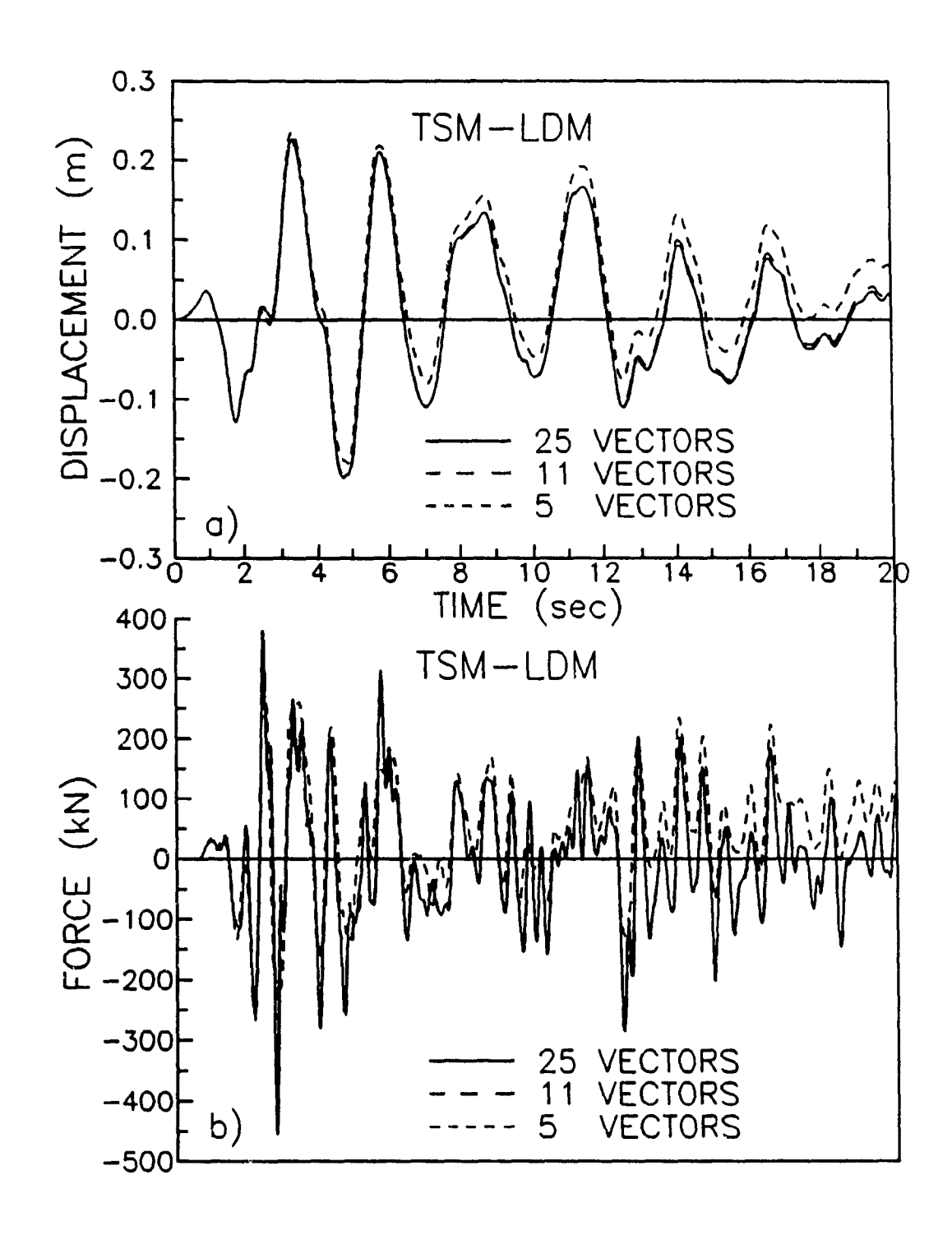


Figure 5.3. Time-history of displacement and force responses for the 25-story building using the TSM-LDM with 25, 11, and 5 vectors.

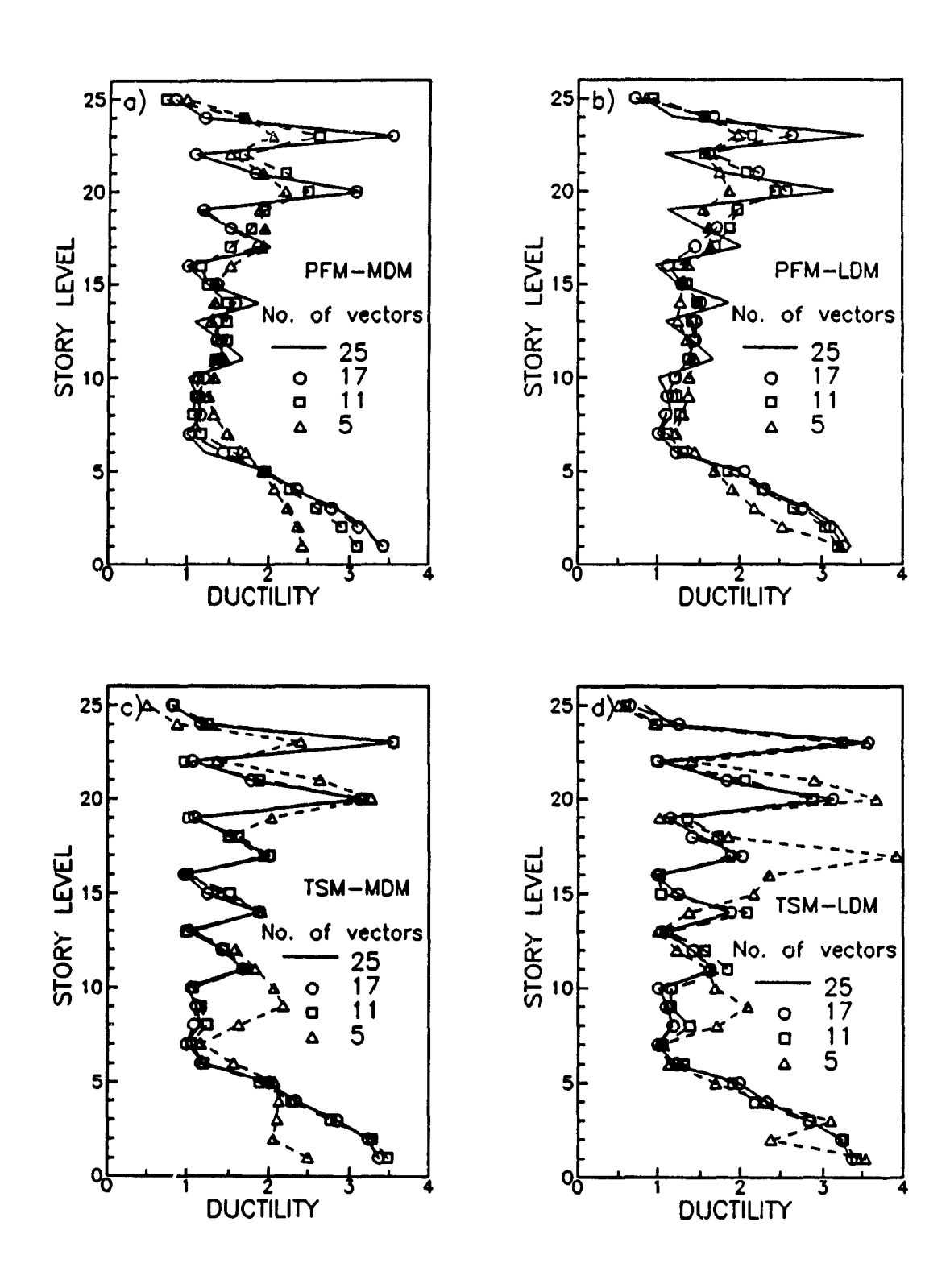


Figure 5.4. Effect of the number of transformation vectors on the peak ductility demand in each story for different solution strategies - 25-story building.

Figure 5.5 shows the convergence of nonlinear response indicators for different solution strategies. For the ductility, μ , the total hysteretic energy, $E_{\rm H}$, and the damping energy, $E_{\rm O}$, dissipated at the end of the earthquake, the results are given in terms of the relative error with respect to the solution using a complete basis. For the error in inergy balance, EEB, the maximum value of Eq. 4-12 multiplied by 100% is used. Figure 5.5a shows the convergence of the ductility demand in level 20 that is representative of the response in the upper region of the building. For solutions using from 5 to 17 vectors, the type of vectors considered does not influence significantly the results. For the PFM-MDM, 17 eigenvectors produce an error of 1 % while 25 vectors are required to get the same accuracy by the PFM-LDM. For a story level representative of the bottom part of the structure, opposite results are observed as shown in Figures 5.4a and 5.4b.

Figure 5.5b indicates that E_H is not sensitive to modal truncation if the TSM is used. The E_H error is larger when the PFM is used instead of the TSM although the values remain below 10% for any solution considering more than 5 vectors. Figure 5.5c shows the error in energy dissipated by viscous damping. The behaviour of the PFM and TSM solutions are very different in the case of the TSM, the computation of the acceleration vector from equilibrium condition introduces a significant error in the acceleration and velocity when a relatively small number of vectors is used. A solution using 17 vectors provides an E_D error below 10% using either vector bases. When the PFM is used, the E_D error is not sensitive to basis truncation since there is no change of basis. Figure 5.5d indicates that the EEB error follows the convergence pattern of the E_D error. A value smaller than 5% should be obtained to ensure a reliable global performance of a particular solution strategy. However, this does not guarantee accurate results for local response indicators such as story ductility demand. Contrary to elastic analyses, the criterion of 95% effective modal mass to obtain a reliable global response is found inapplicable to elastoplastic systems.

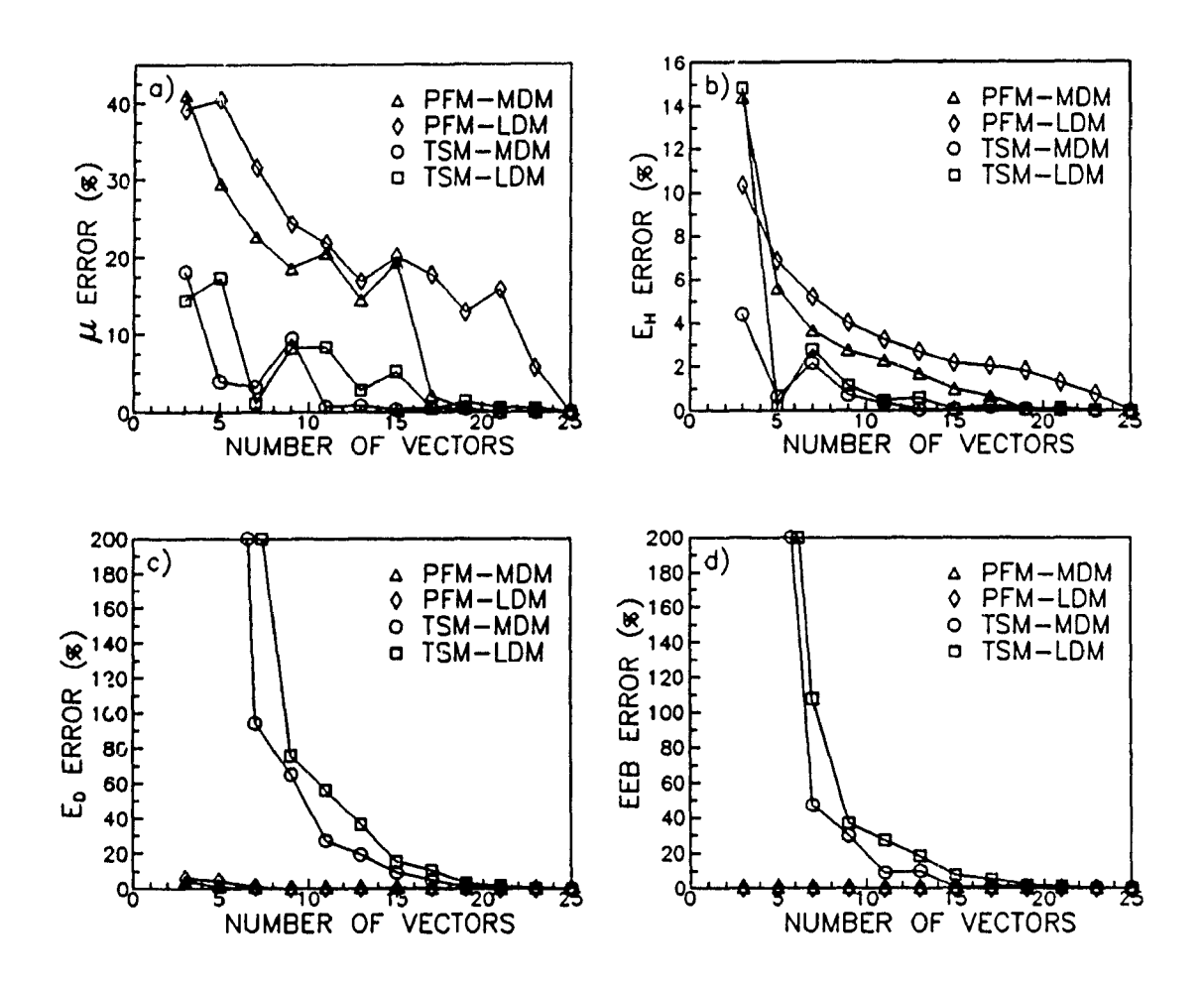


Figure 5.5. Convergence of various nonlinear response indicators for different solution strategies - 25-story building.

5.2.2 Convergence of nonlinear response indicators - 5-story building

Figure 5.6 describes the effect of the number of transformation vectors on the peak ductility demand for different solution strategies applied to the 5-story building. The results indicate that the ductility response is not very sensitive to vector basis truncation when the PFM is used. It should be noted that this method misses all the peaks in ductility demand for the 25-story building and that for this fairly rigid structure there is no sharp peak in story ductility demand. The PFM-LDM produces accurate results considering only 2 vectors in the basis. Figures 5.6c and 5.6d show the very poor behaviour of the TSM for short-period structures.

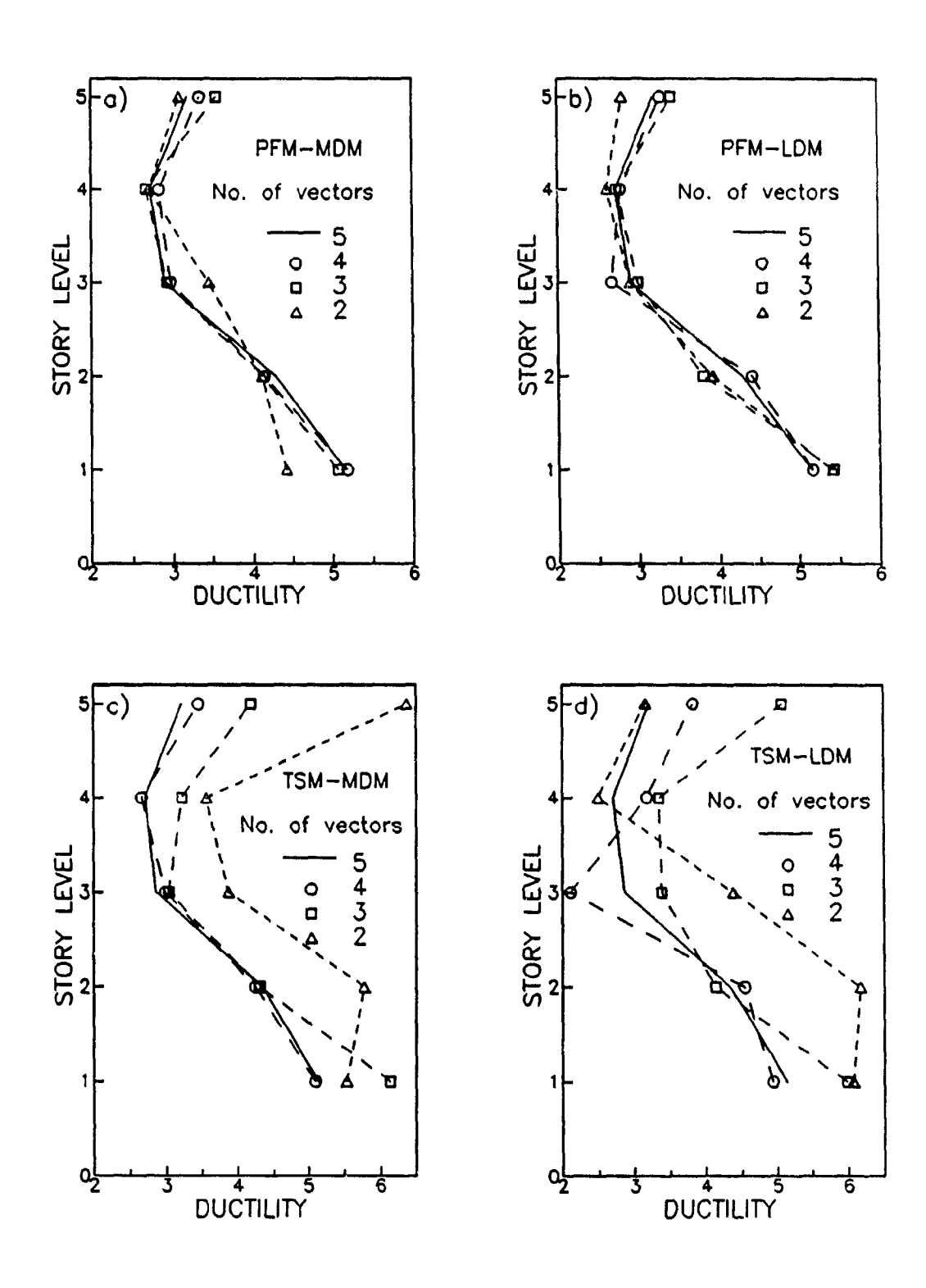


Figure 5.6. Effect of the number of transformation vectors on the peak ductility demand in each story for different solution strategies - 5-story building.

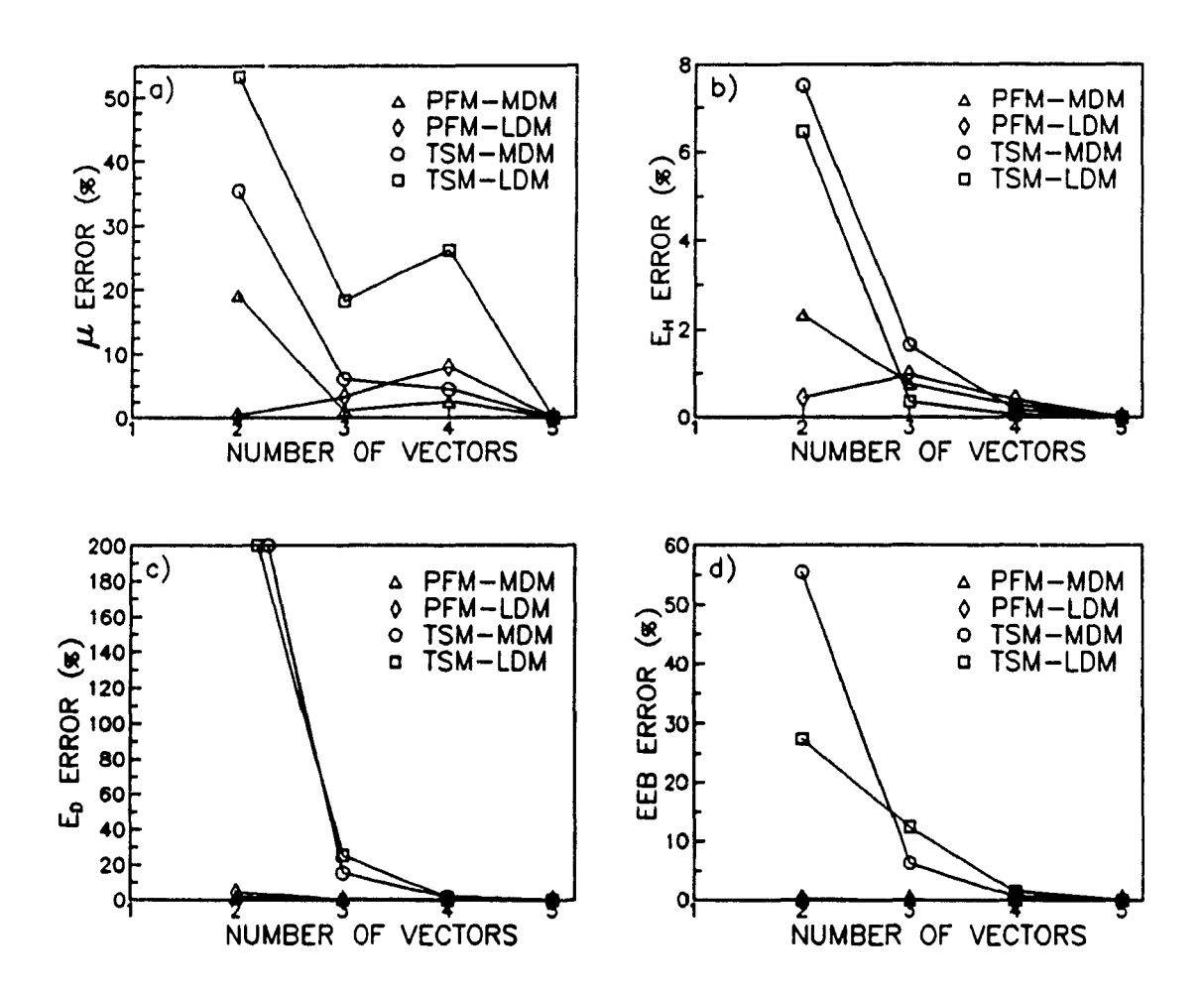


Figure 5.7. Convergence of various nonlinear response indicators for different solution strategies - 5-story building.

Figures 5.7a and 5.7c indicate that for stiff low-rise structures a nearly complete vector basis should be considered to obtain accurate results using the TSM. Figures 5.7b, 5.7c and 5.7d show similar trends to those observed for the 25-story building.

5.3 CONCLUSIONS

In this chapter, the performance of the Pseudo-Force Method (PFM) and the Tangent Spectrum Method (TSM) have been investigated for inelastic seismic response analysis of MDOF structures. The mode displacement (MDM) and the load dependent method (LDM) have been

used in comparative analyses. A flexible 25-story, and a stiff 5-story buildings with bilinear hysteretic behaviour have been considered. The emphasis has been put on the evaluation of ductility demand and energy indicators that are considered for seismic damage evaluation.

For the flexible 25-story building, the TSM can evaluate the peak ductility demand within 10% of the "exact" results using 11 vectors with either the MDM or the LDM. However, the incompatibility between old and updated truncated vector bases requires the computation of the acceleration vector from the equilibrium condition at the end of each time-step. This correction ensures numerical stability of the solution, but the velocity and acceleration can still be inaccurate. Seventeen vectors should then be considered to obtain an error level below 10% on the damping energy and energy balance. The equilibrium iterations are found to be very important to provide a good convergence of the response with a large time-step thus minimizing the number of basis updates. The LDM should be used since the computational effort to generate transformation vectors is much less than that required to generate eigenvectors (MDM).

The PFM is more stable, and requires much less computational effort than the TSM. However, it can not provide any information on the evolution of tangent modal properties in time. For a flexible structure, the ductility demand computed from the PFM is found more sensitive to basis truncation than those computed from the TSM. However, the opposite behaviour is observed for the stiff, 5-story structure, where the TSM is found very sensitive to basis truncation. In this case, results within 10% of the "exact" solution can be obtained from the PFM with a basis of two load-dependent vectors.

Although the PFM is much more computationally effective than the TSM, recent advances in computer vectorization/parallelization of solution algorithms make this solution technique possible on larger systems than those considered in this study. The TSM might

emerge as a valuable tool in earthquake engineering to further improve the understanding and rationalize in a linear format complex nonlinear response mechanisms.

CHAPTER 6

MATHEMATICAL MODELS FOR VISCOUS DAMPING

This chapter describes different mathematical models of viscous damping suitable for nonlinear seismic response analysis. Eight damping models are derived from Rayleigh type damping formulation.

6.1 INFLUENCE OF VISCOUS DAMPING ON ENERGY ABSORPTION

The seismic input energy imparted to a structure is equal to the sum of the kinetic energy, the strain energy, the energy dissipated by hysteretic action of the structural elements, and by other non-yielding mechanisms usually represented by equivalent viscous damping. It is generally postulated that a structure can survive major earthquakes if the structural energy absorption capacity is greater than the seismic input energy (Kuwamura and Galambos 1989, Housener and Jennings 1977). The seismic energy dissipation and related damage models of SDOF systems have been studied by many researchers (Conte et al. 1990, Fajfar and Fishinger 1990, Fajfar et al. 1989, McCabe and Hall 1989, Wu and Hanson 1989, Hadidi-Tamjed 1988, Tembulkar and Nau 1987). Most seismic codes are using force modification factors, that reflect the capability of MDOF structure to dissipate energy through inelastic behaviour, to reduce the seismic forces obtained from linear elastic design procedures. This philosophy generally implies that significant structural and economic damages will be incurred. Zahrah and Hall (1984) have observed that damping has little effects on the amount of energy imparted to a structure by an earthquake, and that damping significantly influences the amount of hysteretic energy available for damage. Various devices have been proposed to increase significantly the effective damping of building structures to limit or eliminate seismic structural damages (Pall and Marsh 1982).

The effect of viscous damping on the seismic response will be influenced by the mathematical model selected for its representation. The damping can be modelled using mass proportional, stiffness proportional or Rayleigh damping computed either from the initial elastic or the tangent inelastic system properties. Otani (1980) compared the experimental nonlinear seismic response of a three-story small-scale reinforced concrete structure with the response obtained from numerical models. Damping matrices proportional to the mass and to the instantaneous stiffness matrices were used with the proportionality coefficients computed from the initial elastic properties. A fair agreement between the experimental results and the numerical results using either damping model, was obtained for the large-amplitude displacement oscillations at the roof. For low-amplitude oscillations, the stiffness proportional damping model provided better correlations with the experimental results.

6.2 DAMPING MATRIX FORMULATION

30

The effects of non-yielding energy dissipation mechanisms are typically represented in MDOF structures by viscous modal damping ratios varying between 0.1% to 7% critical. Because the nature of damping is difficult to quantify analytically, experimentation is used to determine the damping characteristics inherent to various types of structures. Note that damping is often increased in linear analysis to approximate energy losses due to anticipated inelastic behaviour. These increased damping values should not be used in rigorous nonlinear analysis since some losses will be counted twice. The following Rayleigh-type damping representation is used extensively for the linear and nonlinear analyses of MDOF systems (Gillies and Shepherd 1983; Kanaan and Powell 1973):

$$[C]_{t} = a \cdot [M] + b \cdot [K]_{t} + b_{0} \cdot [K]_{t}$$
 (6-1)

where $[C]_t$ is the tangent damping matrix, [M] is the mass matrix, $[K]_t$ is the tangent stiffness matrix, and $[K]_t$ is the initial stiffness matrix. The coefficients a, b, and b₀ are proportionality

constants computed from the natural frequencies of the structure. If a, or b and b_0 are set to zero, stiffness or mass proportional damping are obtained, respectively. In linear analysis, b=0, and Eq. 6-1 allows to control a specified damping ratio, ξ , at two distinct frequencies ω_1 and ω_2 as shown in Figure 6.1. The coefficients a and b_0 are computed from:

$$\mathbf{a} = \frac{\mathbf{a} \cdot \mathbf{\xi} \cdot \mathbf{\omega}_i \cdot \mathbf{\omega}_l}{\mathbf{a} + \mathbf{\omega}_l} \tag{6-2}$$

$$b_0 = \frac{2 \cdot \xi}{\omega_I + \omega_I} \tag{6-3}$$

In Eqs 6-2 and 6-3, ω_i is usually taken as the first natural frequency and ω_j is the frequency of the highest mode that contributes significantly to the response. The value of ω_i is often taken as the frequency for which 90% to 95% of effective modal mass is represented by a truncated vector basis. In nonlinear analysis, the following methods can be used to obtain [C],:

M1: the coefficients a and/or b_0 are computed from the initial elastic frequencies with b=0, this results in a time independent damping matrix. The following notation is used to describe variations among this model; M1(a), M1(b_0), M1(a_1b_0). The coefficients in parentheses indicate which terms of Eq. 6-1 are retained in the formulation.

M2: the coefficients a and b are computed from the initial elastic frequencies with $b_0=0$, this results in a time dependent damping matrix since $[K]_t$ is changing with time. The possible models are M2(b), M2(a,b).

M3: the coefficients a and/or b are computed from the tangent frequencies with $b_0=0$, this results in a time dependent damping matrix and constant damping ratio for the modes used to compute the coefficients a and b. The possible models are M3(a), M3(b), and M3(a,b). The subscript t is added to a and b to indicate clearly that these coefficients are computed from tangent free-vibration properties that are continuously changing when the response is inelastic.

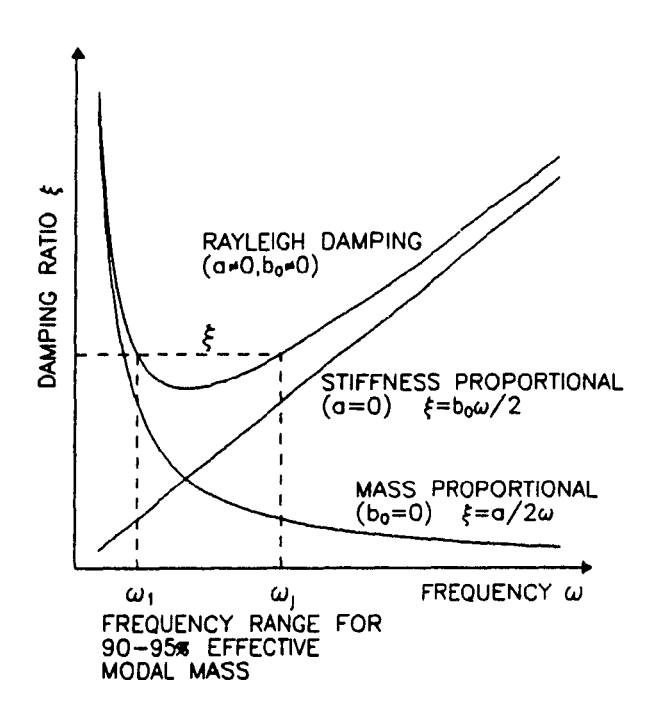


Figure 6.1. Rayleigh damping.

For example, Otani (1980) used the M1(a) and M2(b) damping models in the seismic analysis of reinforced concrete buildings as mentioned previously. Schiff et al. (1991) used Rayleigh damping proportional to [K]_{tt} the M2(a,b) model, to study the nonlinear response of low-rise steel moment resisting frames. Filiatrault (1990) used mass proportional damping, the M1(a) model, to study the seismic response of MDOF wood structures with nonlinear connectors. Sedarat and Bertero (1990) used Rayleigh damping proportional to the initial system matrices, the M1(a,b₀) model, to study the nonlinear torsional response of MDOF concrete structures. El-Aidi and Hall (1989) used the stiffness proportional damping model, M2(b₀), to study the nonlinear response of concrete dams. In all cases reported in the literature, the damping proportionality coefficients were computed from the initial elastic free-vibration properties.

The classical integration procedures used in nonlinear seismic analysis correspond to the simultaneous integration of all modes of vibration at a particular time-step. The actual (instantaneous) frequencies of the system are continuously changing during nonlinear behaviour. The response of the system may thus be obtained in terms of the nonlinear (tangent stiffness) frequency spectrum (Idelsohn and Cardona 1985, Gillies and Shepherd 1983, Bathe and Gracewski 1981, Nickell 1976). The use of the initial elastic frequencies to compute the damping proportionality coefficients comes mainly from computational conveniences since the evolution of the frequency spectrum of the dominating modes throughout the nonlinear response is usually unknown. In the analysis of softening structures (elasto-plastic condition), the frequencies become smaller when the structure experiences nonlinear behaviour. The selected frequencies based on linear analysis to compute Rayleigh damping coefficients may thus cover a too narrow range. The use of tangent spectrum properties will therefore permit a more rational control of the amount of energy dissipated by viscous damping in nonlinear seismic analysis.

CHAPTER 7

SEISMIC ENERGY DISSIPATION IN MDOF STRUCTURES

7.1 INTRODUCTION

The influence of viscous damping models on the nonlinear energy response of MDOF structures has not received a lot of attention in the past. The purpose of this chapter is to investigate the displacement ductility demand, indices related to the relative amount and rate of energy dissipation, and the number of yield excursions of MDOF using mass and/or stiffness proportional damping models. Solution strategies using initial elastic or tangent inelastic structural spectrum properties are used to evaluate the damping matrices. Bilinear hysteresis models of simple MDOF structures presented in chapter 4 with different strength levels, strain hardening ratios, and damping ratios are considered.

The computer program presented in chapter 2 is used to perform the step-by-step integration of the equations of dynamic equilibrium using either geometric coordinates or modal coordinates. When modal coordinates are used, the frequency and mode shapes are computed from the tangent stiffness at each time-step. The equations of motion are then transformed and solved in generalized coordinates. A complete eigenbasis is used in all computations. This is to avoid any error in the nonlinear response indicators due to modal truncation thus maintaining a computational strategy equivalent to a step-by-step integration in geometric coordinates.

7.2 INFLUENCE OF DAMPING MODELS ON SEISMIC RESPONSE

The influence of the eight damping models described in chapter 6 is first investigated for the 10-story building with the force modification factor, R=4, the strain hardening ratio, α =1%, and the damping ratio, ξ =5%, subjected to the three selected earthquakes.

7.2.1 Evolution of nonlinear tangent properties

Figure 7.1a shows the variation in the fundamental period of vibration due to inelastic behaviour. The instantaneous period of the first mode increased from 1 sec for elastic response to a maximum of approximately 8 sec when the system responded inelastically. Figure 7 1b indicates the variations in the number of modes required to maintain 95% of effective modal mass in the solution. For the elastic response, modes 1 to 4 should be included. For inelastic response, this range increased to modes 1 to 10, or the complete eigenbasis. However, the first five modes are found adequate for almost the entire nonlinear analysis except for three very short periods of time.

Figure 7.2 shows the variation of the Rayleigh damping coefficients to maintain 5% instantaneous critical damping using the tangent damping model, M3(a,b). The damping coefficients, a, b, are computed using the first tangent frequency and the tangent frequency of the highest mode required to obtain 95% effective modal mass in the solution. If only mass proportional damping is considered (M3(a)), the damping ratio can be as low as 0.2% in the highest mode required to obtain 95% effective modal mass. On the other hand, the damping ratio in this mode can be as high as 217% if only stiffness proportional damping is considered (M3(b)). The seismic response using the damping model M3(b) will thus be significantly overdamped.

7.2.2 Displacement responses at the top

Figure 7.3 shows the top displacement responses for the 10-story building subjected to the El Centro earthquake. The mass proportional and the Rayleigh damping models using either the initial elastic or the tangent inelastic damping coefficients yield almost identical results. The stiffness proportional damping models show significant variations in the displacement responses. The damping model using tangent properties, M3(b_i), provides the largest damping, followed respectively by the initial elastic, M1(b₀), and the instantaneous stiffness proportional, M2(b), damping models. When Rayleigh damping is used, the dispersion observed in the stiffness proportional damping models is significantly reduced. In this case, the mass component of the damping appears to dominate the response.

7.2.3 Nonlinear response indicators

Figure 7.4 shows the variation in the nonlinear response indicators due to the use of different damping models for the 10-story building subjected to the three earthquake records. Consistent variations are obtained from the different damping models as different earthquake records are considered. The tangent damping models using mass proportional, M3(a), and stiffness proportional, M3(b), damping, respectively produce about the highest and lowest intensity of the nonlinear response indicators. If these models are excluded from the analyses, average relative variations among the remaining damping models of about 40%, 20% and 80% are respectively observed for the average ductility, E,/E, ratios, and the average number of yield excursions. If only the three types of Rayleigh damping models are considered, M1(a,b₀), M2(a,b), and M3(a,b₀), the average relative variations of the same response indicators are respectively reduced to 10%, 8% and 30%. The average number of yield excursions is therefore more sensitive to the earthquake records and damping models than the average ductility and the E,/E, ratio.

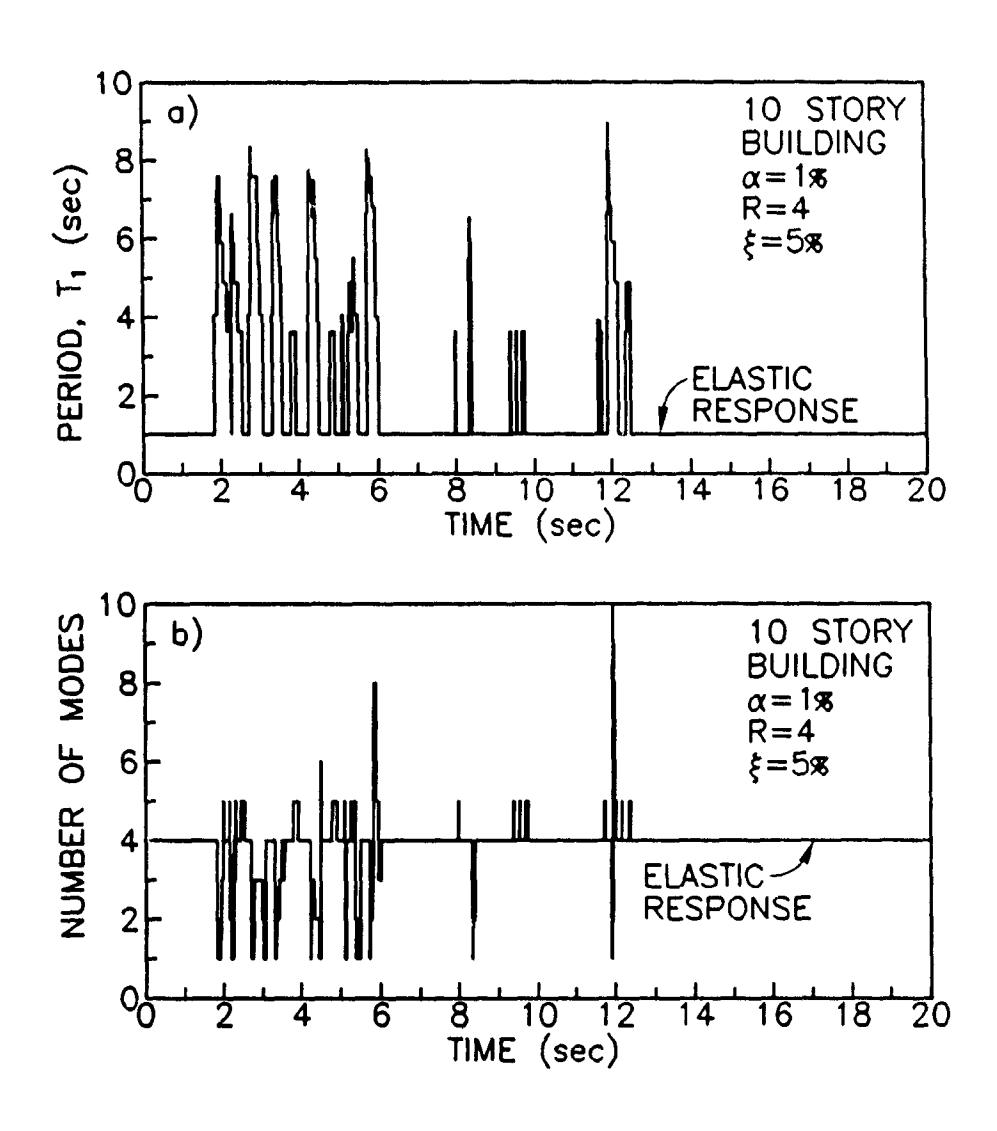
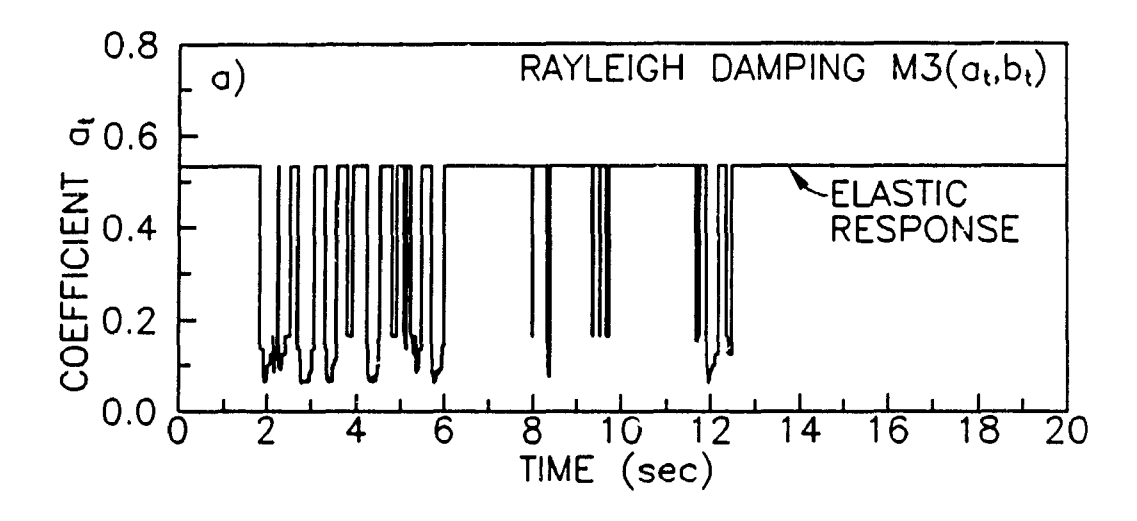


Figure 7.1. Evolution of tangent modal properties using damping model M3(a,,b) for the 10-story building subjected to El Centro earthquake (R=4, α =1%, ξ =5%), a) period of the first mode, b) number of modes for 95% of effective modal mass.



ş

1

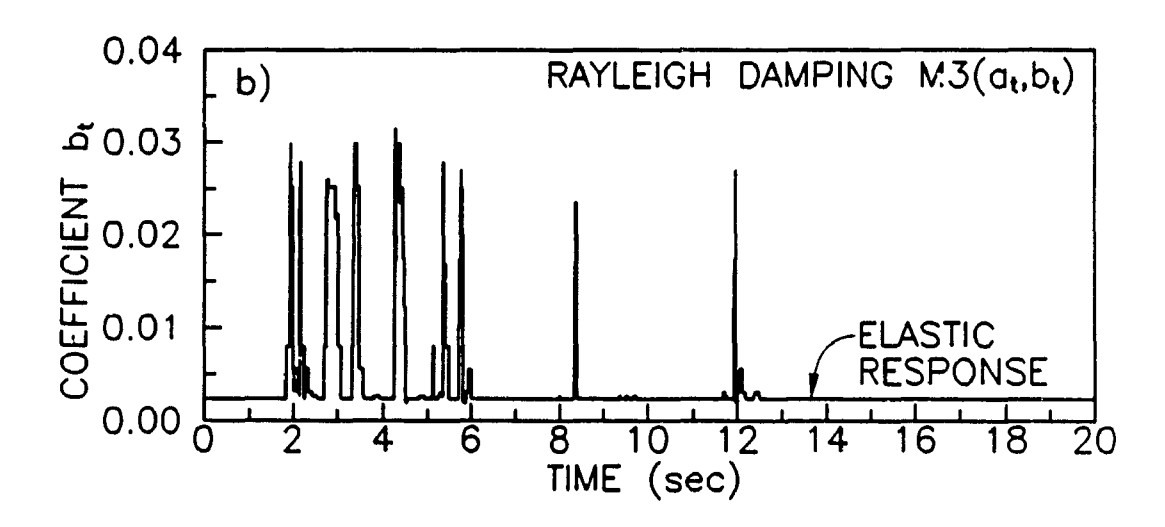


Figure 7.2. Evolution of the Rayleigh damping coefficients using damping model M3(a,b) for the 10-story building subjected to the El Centro earthquake (R=4, α =1%, ξ =5%).

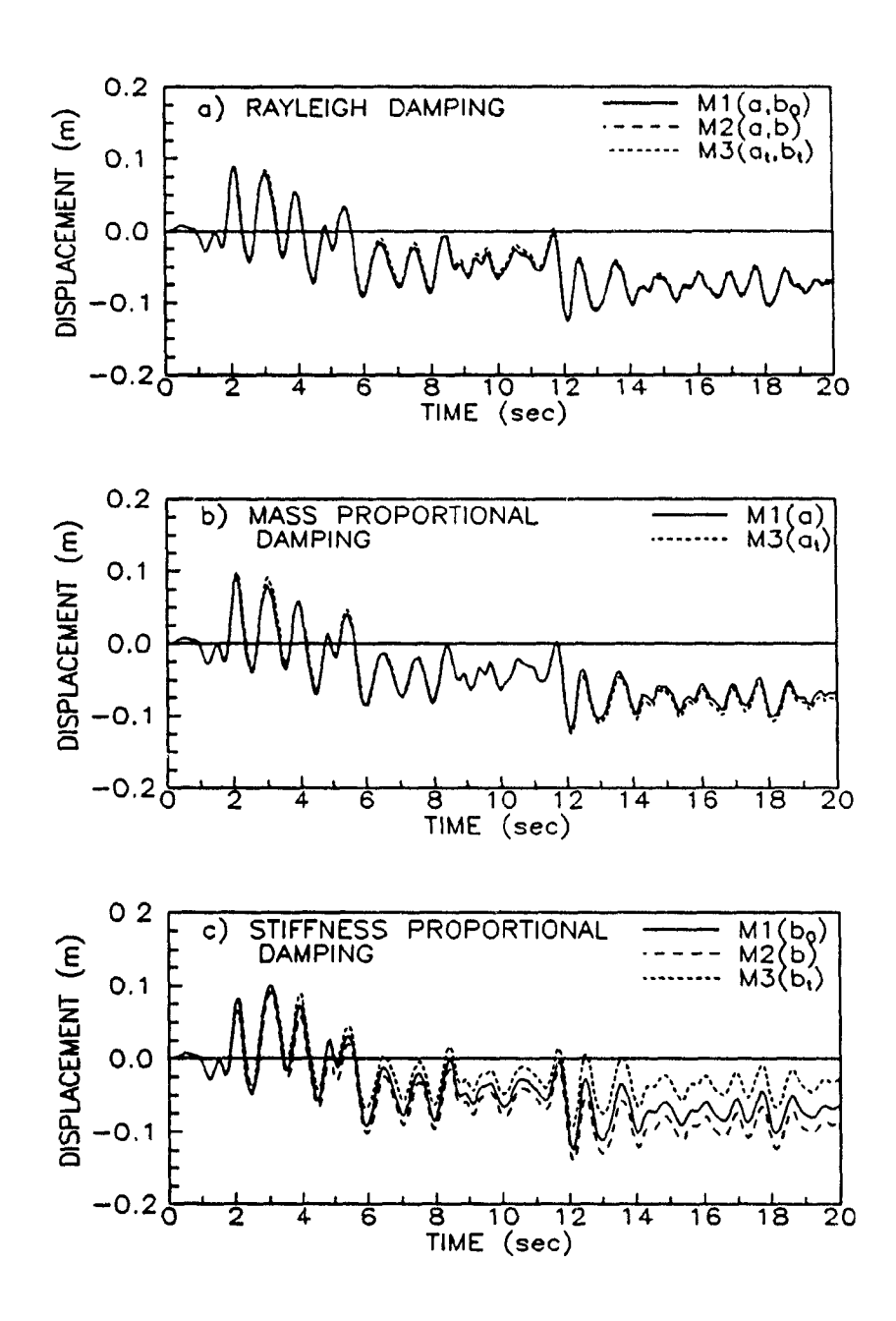


Figure 7.3. Top displacement of the 10-story building subjected to the El Centro earthquake for various damping models (R=4, α =1%, ξ =5%).

Figure 7.5 shows the variations in the power response indicators due to different damping models for the 10-story building subjected to the three earthquake records. Consistent variations are also observed from the different damping models as different earthquake records are considered. The most sensitive response parameters to the type of damping model are respectively the damping power, P_D, the input power, P_I, and the hysteretic power, P_H. If the mass and stiffness tangent damping models are excluded from the analyses, average relative variations of about 40%, 10% and 5% are obtained among the remaining damping models for P_D, P_I, and P_H, respectively. These variations do not change significantly if the comparisons are restricted to the three Rayleigh damping models. For a given earthquake, the rate of hysteretic energy dissipation is not very sensitive to the selected damping model.

7.3 PARAMETRIC STUDY

A parametric study is performed by considering for the seven buildings subjected to the EI Centro earthquake, the three Rayleigh damping models and the instantaneous stiffness damping model, M2(b), with b computed from the initial elastic properties. Rayleigh damping is commonly used in practice, and the model M2(b) has been shown by Otani (1980) to provide a good correlation with experiments for low-rise reinforced concrete buildings designed with a strength parameter, η =0.5. Two values of the damping ratio, ξ (2%, 5%), of the force modification factor, R (2, 4), and of the strain hardening parameter, α (1%, 25%), are considered in the parametric study. The average ductility, the average number of yield excursions, the ratio E_H/E_H and the maximum value of hysteretic power, P_H , are computed in each case. With the exception of E_H/E_H the nonlinear response indicators are very high for the single story (SDOF) building (T₁ = 0.1 sec) as compared with the MDOF buildings. For the SDOF building, the numerical values of these indicators have thus been reported in parenthesis beside each damping model in the figure legends.

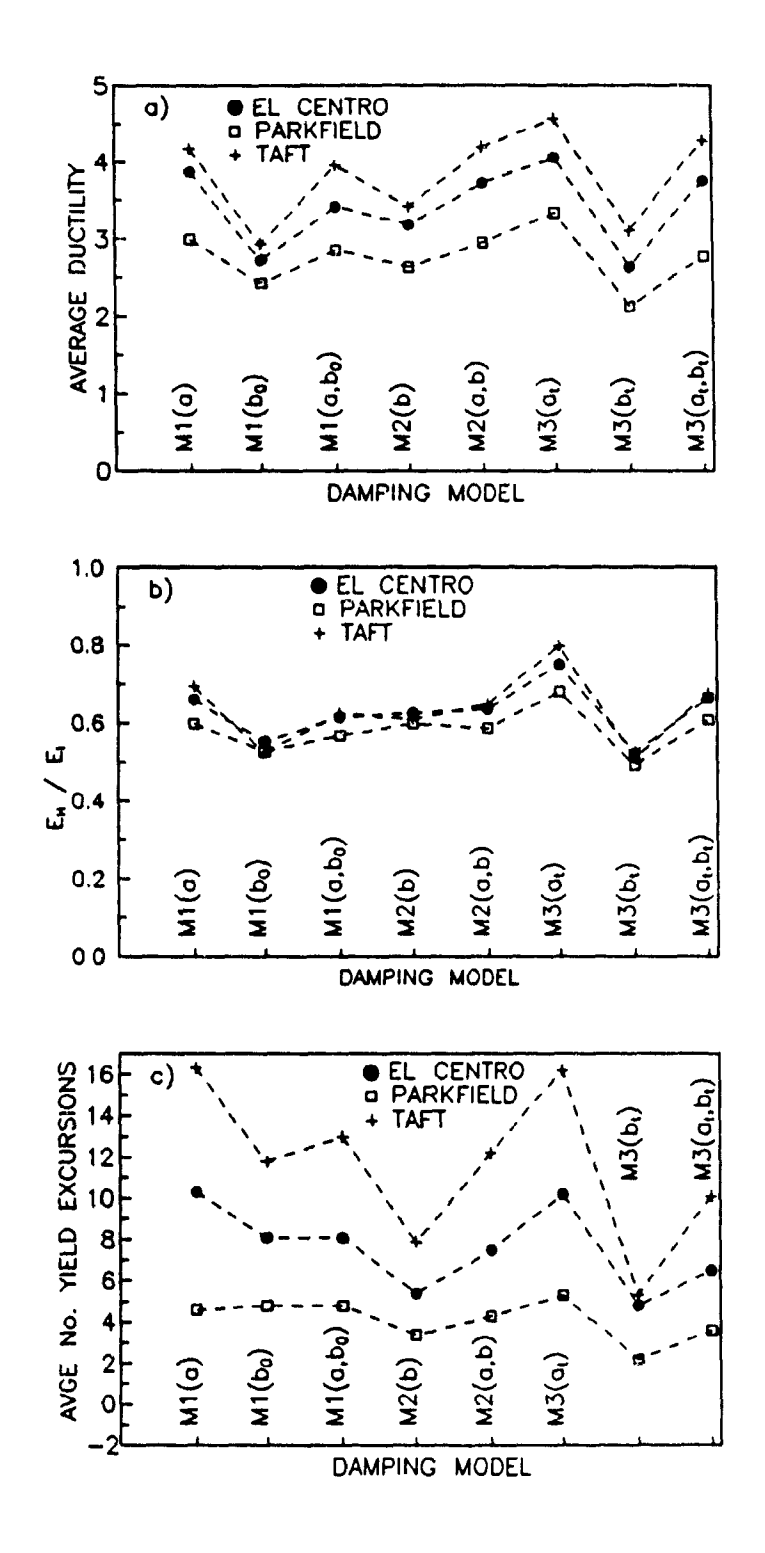


Figure 7.4. Nonlinear response indicators for the 10-story building for various damping models (R=4, α =1%, ξ =5%).

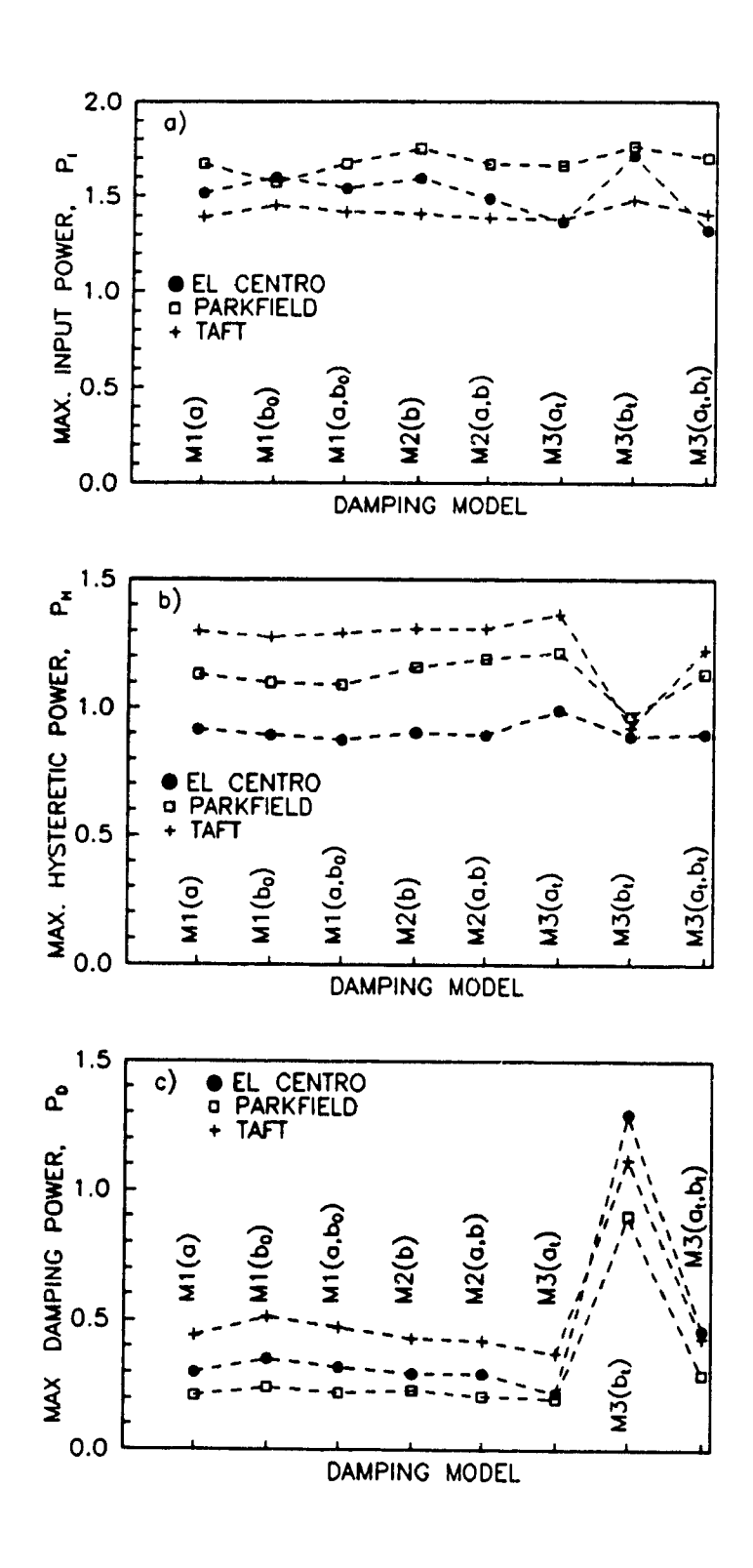


Figure 7.5. Power response indicators for the 10-story building for various damping models (R=4, α =1%, ξ =5%).

T.

The tangent Rayleigh damping model, M3(a,,b), is using proportionality coefficients that are updated at each time-step. It maintains throughout the elastic and inelastic response, a constant damping ratio for the first mode, and the mode required to obtain 95% of effective modal mass. This approach provides a rational control of the viscous damping mechanism in nonlinear seismic analyses as initially selected by the analyst. The M3(a,b) model will thus form the basis upon which the performance of the other damping models will be compared.

7.3.1 influence of damping ratio

Figure 7.6 shows the effect of the pamping ratio on the nonlinear response of multistory buildings. A reduction in the damping ratio from 5% to 2% increases the intensity of all nonlinear response indicators. Considering the tangent Rayleigh damping model, M3(a,b), it is shown in Figure 7.6c that for $T_1 \ge 1.5$ sec, the E_H/E_I ratio is approximately constant. In this range, the ratio E_H/E_I increases from 0.55 for $\xi = 5\%$ to 0.75 for $\xi = 2\%$. This represents an increase of about 35% of the hysteretic energy available for damage. In the short period range $(T_1 \le 0.5 \text{ sec})$, the influence of damping on E_H/E_I ratios is not as significant. Increases of about 15% are now observed when ξ is reduced from 5% to 2%. For $T_1 \le 0.5$ sec, the E_H/E_I ratios computed from the stiffness proportional damping model, M2(b), are almost identical with the rigorous M3(a,b) damping model. For $T_1 > 0.5$ sec, the M2(b) model dissipates more energy by viscous damping than the Rayleigh models, producing smaller E_H/E_I ratios. For $T_1 \ge 1$ sec, the Rayleigh model using the instantaneous stiffness, M2(a,b), yields E_H/E_I ratios that are within 4% of the values computed from the tangent Rayleigh damping model, M3(a,b). In this range, the Rayleigh damping model based on initial system matrices, M1(a,b_o), provides E_H/E_I ratios that are within 10% of the M3(a,b) damping model.

Figure 7.6a indicates that a reduction of ξ from 5% to 2% increases the average ductility demand by about 15% over the complete range of fundamental periods. The influence of the

various damping models on the average ductility is similar to the effects observed for the E_H/E_1 ratios. Figure 7.6b indicates that the average number of yield excursions decreases rapidly as T_1 increases. For structures with $\xi = 5\%$ and $T_1 \le 0.5$ sec, the average number of yield excursions is not sensitive to the damping model selected. For systems with $T_1 > 0.5$ sec, the M2(b) damping model underestimates the average number of yield excursions. As ξ is reduced from 5% to 2%, the M2(b) damping model underestimates the average number of yield excursions over a wider range of fundamental periods corresponding to $T_1 > 0.1$ sec. Figure 7.6d indicates that the maximum hysteretic power, P_H , is also decreasing very rapidly as T_1 increases. For $T_1 \ge 0.5$ sec, P_H is not sensitive to the values of ξ and the damping models. For $T_1 < 0.5$ sec, significant variations are observed among the values computed from the different damping models. In this range, the stiffness proportional damping model, M2(b), shows again an excellent correlation with the rigourous tangent Rayleigh damping model M3(a,b).

7.3.2 influence of force reduction factor

Figure 7.7 shows the effect of the force reduction factor on the nonlinear response of multistory buildings. Figure 7.7a indicates that for the 10 story building (medium period range) designed with R=4, an average ductility demand equal to 3.75 is obtained from the tangent Rayleigh damping model, M3(a,b). This value is within 6% of the selected force modification factor, R=4. The parameter R can thus be interpreted as a global ductility factor for MDOF structures in the medium period range. For short-period structures designed with a substantial force modification factor, given here by R=4 and $\eta \le 1$, the ductility demand is very high as the period is reduced and the systems converge toward the static response. For the structures designed with R=2, the parameter η is larger than 1 for T₁ < 0.5 sec. In this case, the average ductility will converge to the selected value of R=2 as the period is reduced.

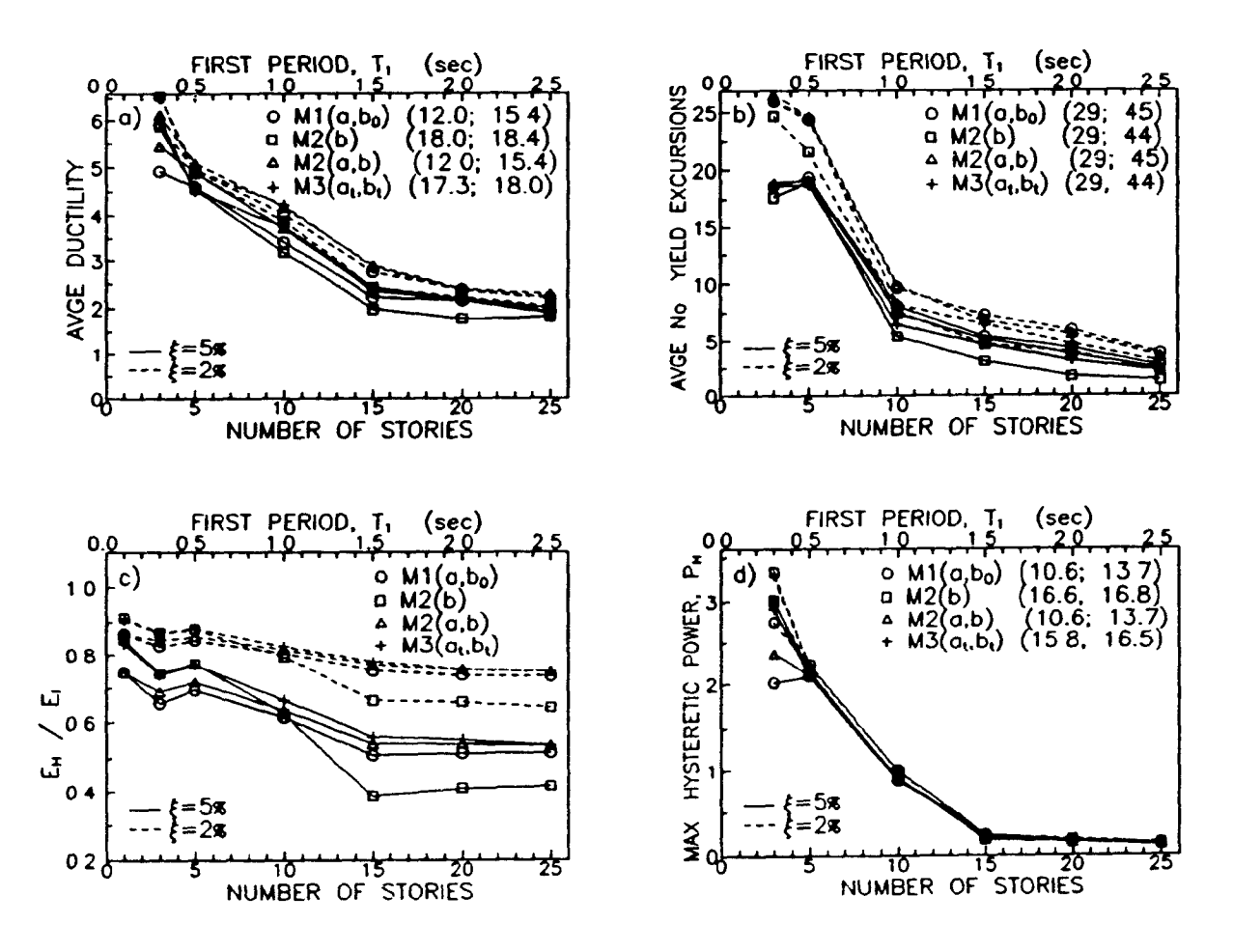


Figure 7.6. Influence of the damping ratio, ξ , on the response of multistory buildings (R=4, α =1%) subjected to the El Centro earthquake

The average ductility and the E_{tr}/E_{t} ratio are not sensitive to the damping models for structures with $T_{t} < 1.0$ sec designed to respond with mild inelastic behaviour as given by R = 2. For structures with $T_{t} > 1.0$ sec, the M2(b) model should not be used since it overdamps the energy response significantly.

Figure 7.7b indicates that if the M2(b) damping model is excluded, the average number of yield excursions is not sensitive to the Rayleigh type of damping model selected for R=2. Figure 7.7d indicates that in the medium and short-period ranges $(0.1 < T_1 < 1.5 \text{ sec})$ the hysteretic power increases as the force modification factor is reduced from R=4 to R=2. This trend is reversed for $T_1=0.1$ sec. For mildly nonlinear systems (R=2), P_{H_1} is not sensitive to the selected type of Rayleigh damping model over the complete frequency range. The M2(b) model should not be used for $T_1 > 1.0$ sec since it overdamps the P_H response.

7.3.3 Influence of strain hardening ratio

Figure 7.8 shows the effect of the strain hardening ratio, α , on the nonlinear response of multistory buildings. In the short-period range, the average ductility does not exceed about 5 for α =25% as compared to a maximum value of 18 for α =1%. The variations in average ductility among the various damping models is reduced as α is increased from 1% to 25%. For long period structures (T₁ > 1.5 sec), the average ductility is not very sensitive to the strain hardening ratio.

Figure 7.8c indicates that in the short period range ($T_1 < 0.5$ sec), the E_H/E_1 ratio is reduced as the strain hardening is increased. For systems using large α , the M2(b) and M2(a,b) damping models should be used to approximate the response of the tangent Rayleigh damping model, M3(a,b), in the short-period ($T_1 \le 0.5$ sec) and the medium and long period range ($T_1 > 0.5$ sec), respectively. Figure 7.8b indicates that the average number of yield excursions

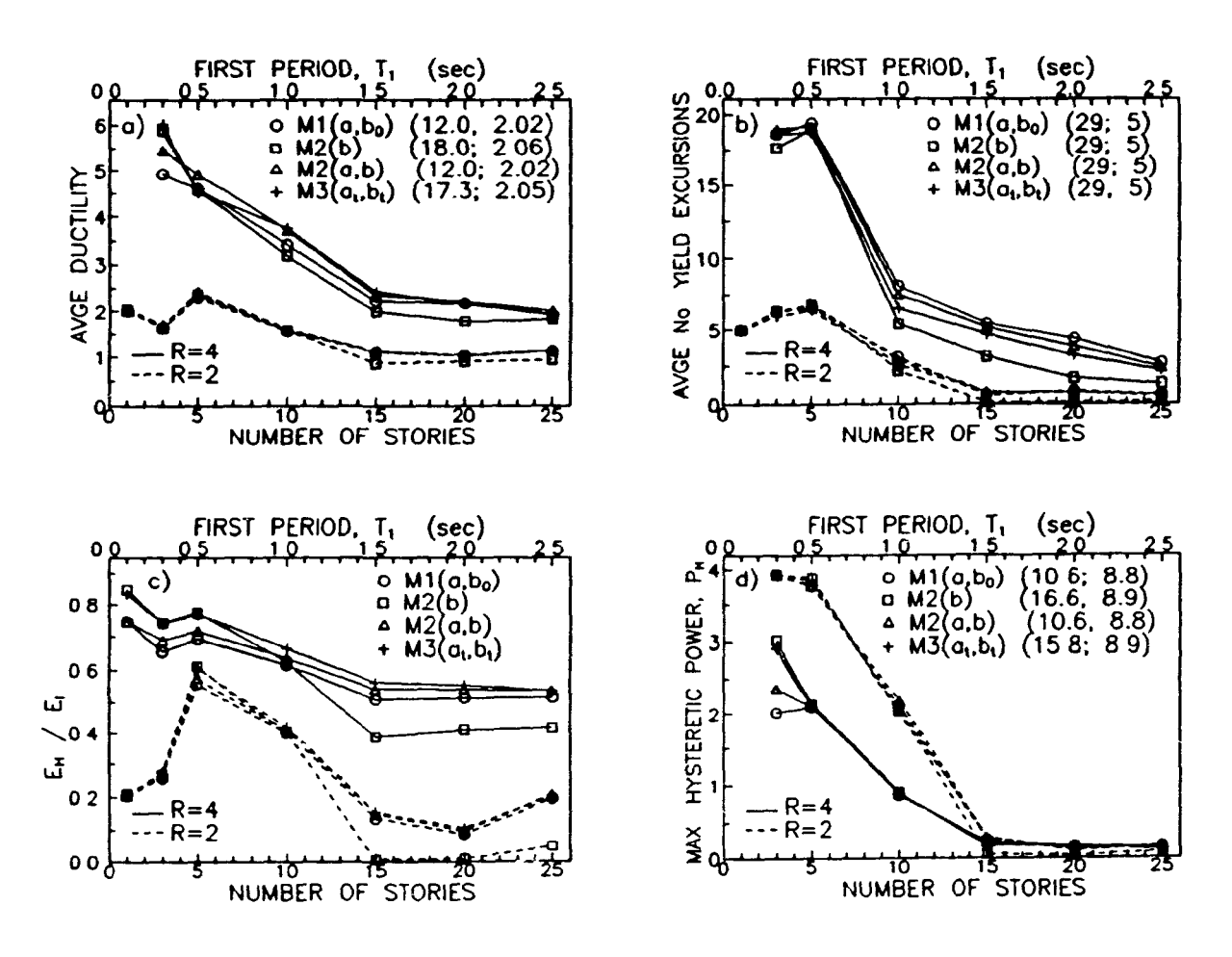


Figure 7.7. Influence of the force modification factor, R, on the response of multistory buildings (ξ =5%, α =1%) subjected to the El Centro earthquake

increases with an increase in the strain hardening ratio. For large α , there is no significant variation of the average number of yield excursions among the Rayleigh damping models, except for the M2(b) model for T₁ > 0.5 sec. Figure 7.8d indicates that the strain hardening does not affect the P_H values for T₁ > 1 sec. For T₁ < 0.5 sec and α =25%, the P_H values exhibit minor variations for the different damping models.

7.4 CONCLUSIONS

In this chapter, the effects of various mathematical models to represent viscous damping in nonlinear seismic analysis of MDOF structures have been investigated. Bilinear hysteretic models of simple MDOF structures using different strength levels, strain hardening ratios, and damping ratios have been considered. The average ductility demand, the average number of yield excursions, the ratio of hysteretic to input energy, $E_{\rm h}/E_{\rm h}$, and the maximum rate of hysteretic energy dissipation have been selected as indicators to characterize the nonlinear seismic response.

A tangent Rayleigh damping model using proportionality coefficients that are updated at each time-step has been developed. It maintains throughout the elastic and inelastic response, a constant damping ratio for the first mode, and the mode required to obtain 95% of effective modal mass. This approach provides a rational and rigorous control of the damping in nonlinear seismic analyses. In practice, the damping proportionality coefficients are usually computed from the initial elastic properties. In this case, damping proportional to the instantaneous stiffness, the M2(b) damping model, should be used for MDOF structures with fundamental periods of vibration, $T_1 \le 0.5$ sec. For the systems analyzed with $T_1 \le 0.5$ sec and the M2(b) damping model, all seismic response indicators were very closed to the tangent Rayleigh damping model for a wide range of damping ratios, strain hardening ratios and force reduction factors. For MDOF structures with $T_1 > 0.5$ sec, Rayleigh damping should be used.



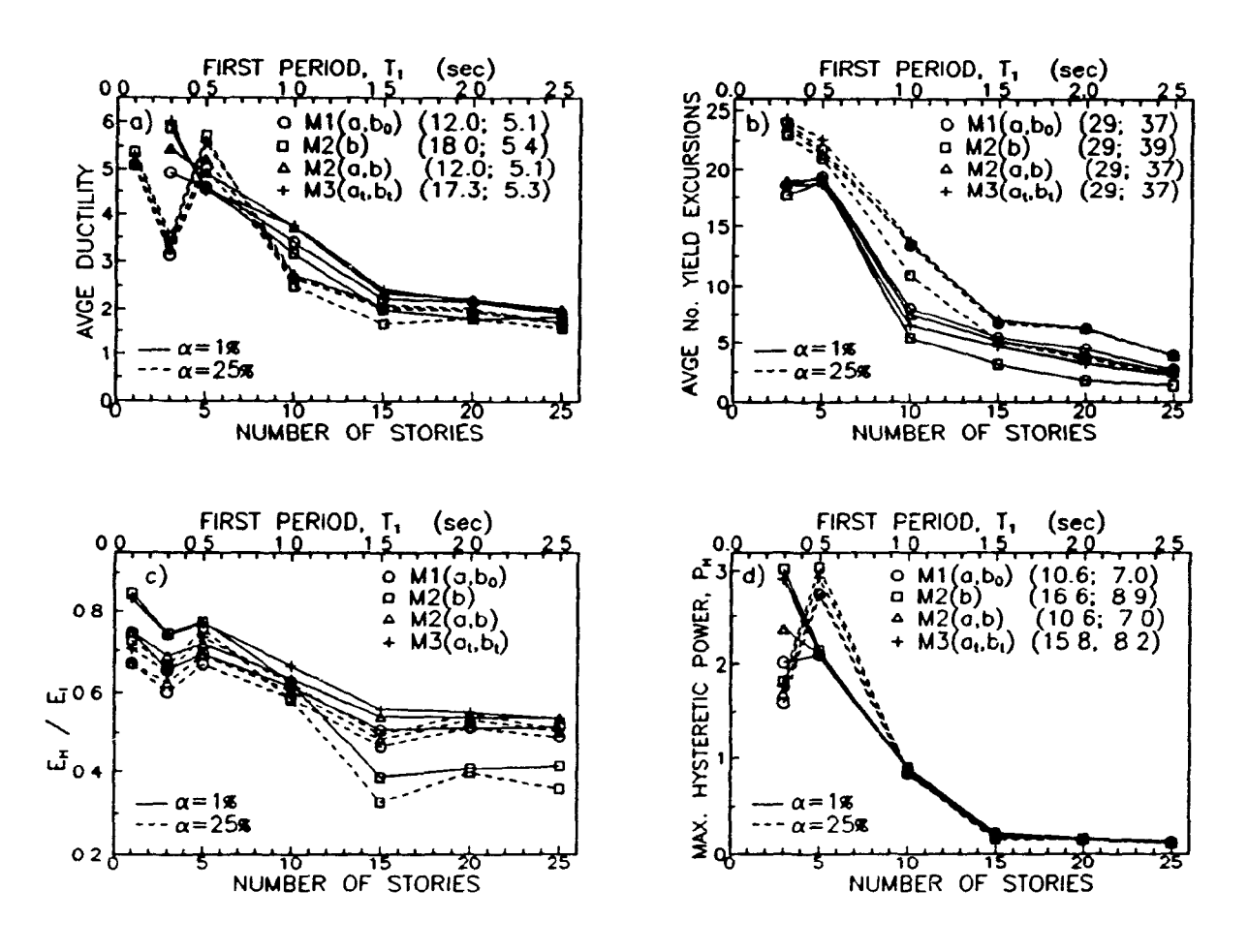


Figure 7.8. Influence of the strain hardening ratio, α , on the response of multistory buildings (R=4, ξ =5%) subjected to the El Centro earthquake.

The Rayleigh damping model using the instantaneous stiffness with the proportionality coefficients computed from the elastic properties provides a very good agreement with the more rigorous tangent damping model in the medium period range (0.5 < T₁ < 1.5 sec). For multistory buildings with T₁ > 1.5 sec, the seismic response is not affected by the type of Rayleigh damping model selected.

CHAPTER 8

CONCLUSIONS

8.1 SUMMARY

This thesis has presented a study of nonlinear seismic response of MDOF structures using vector superposition methods. Bilinear hysteretic models of "shear beam" MDOF structures subjected to three different earthquake records have been considered for parametric studies. The MDOF structures have been designed to meet the requirements of the National Building Code of Canada (NBC 1990) and the earthquake records have been grouped around the NBC 1990 response spectra for building structures located in Victoria B.C. Two distinct investigations have been made. First, the solution algorithms for nonlinear vector superposition analyses have been studied. Second, a comparative study of different mathematical models for viscous damping has been made.

Step-by-step integration of the incremental form of the equations of dynamic equilibrium expressed in geometric coordinates is generally used to investigate the nonlinear elasto-plastic behaviour of MDOF structures. The integration procedure mathematically corresponds to the simultaneous integration of all instantaneous modes of vibration. Chapter 2 presented solution algorithms to use vector superposition methods in nonlinear analysis that consist in performing a change of basis to a more effective system of equations using either the Pseudo-Force Method (PFM) or the Tangent Spectrum Method (TSM). In the PFM, a single set of modes based, on elastic system matrices are employed during the complete response calculation, and the

nonlinearities are taken as pseudo-forces on the right hand side of the equation of motion. In the TSM, the change of basis is performed at each time-step using mode shapes and frequencies corresponding to the instantaneous system matrices.

An investigation of the elasto-plastic seismic response of MDOF structures using the PFM and the TSM has been presented in chapter 5. The emphasis was put on the effect of vector basis truncation on the nonlinear response and the stability of the solution algorithms. An equilibrium correction method has been proposed to provide numerical stability to tangent solutions when truncated vector bases are used. The effectiveness of a new algorithm to generate load-dependent vectors that provides a static correction for the truncation of the higher modes has been evaluated in the context of elasto-plastic analysis. The displacements, the internal member forces, the ductility demand, the hysteretic, and the damping energy dissipated during the nonlinear seismic response, have been selected as indicators to study the convergence characteristics of different solutions strategies.

The seismic input energy imparted to a structure is dissipated by hysteretic behaviour and by other non-yielding mechanisms usually represented by equivalent viscous damping. It is generally recognized that there is a strong correlation between the energy dissipated by hysteretic action and the seismically induced level of damage. While viscous damping has been found to have a small effect on the amount of energy imparted to a structure, it has a significant influence on the amount of hysteretic energy dissipation. A parametric study has been presented in chapter 7 on the influence of the mathematical modelling of viscous damping on seismic energy dissipation of MDOF structures. The damping has been modelled using mass proportional, stiffness proportional, and Rayleigh damping computed either from the initial elastic or the tangent inelastic system properties. Various structural performance indices have been evaluated for bilinear hysteresis model of simple MDOF structures with different strength levels,

strain hardening ratios, and damping ratios.

8.2 CONCLUSIONS

From the results obtained, several conclusions can be reached about the applicability of vector superposition methods and the proper mathematical modelling of viscous damping in nonlinear seismic problems.

8.2.1 Vectors superposition methods

For the applicability of vector superposition methods in nonlinear seismic analyses and the effects of vector basis truncation, the general conclusions can be summarized as follows.

- If the TSM is used, the acceleration vector should be computed from equilibrium condition to account for the incompatibility of an updated basis to fully represent the initial conditions at $t + \Delta t$. The acceleration and velocity can still be in error but the solution will be numerically stable.
- The equilibrium iterations have been found to be very important to provide a good convergence of the response with a large time-step thus minimizing the number of basis updates.
- The displacement response has been shown not reliable to judge of the quality of a solution strategy in nonlinear seismic analysis.
- The use of load dependent vectors (LDM) or eigenvectors (MDM) has not shown significant influences in both PFM or TSM. The LDM should be used since the computational effort to generate transformation vectors is much less than that required to generate eigenvectors (MDM).
- The PFM was more stable, and required much less computational effort than the TSM.
 However, it can not provide any information on the evolution of tangent modal properties in time.

For the investigation on the flexible 25-story building, the main conclusions are:

- Considering the peak ductility demand, the TSM is much less sensitive to the truncation
 of the vector basis than the PFM.
- Considering the peak ductility demand and hysteretic energy dissipation, 11 vectors are required when the TSM is used to have an error level below 10% of the "exact" results.
 However, if the damping energy and the energy balance are considered, 17 vectors are required to maintain the error level below 10%. This is due to the error in velocity and acceleration caused by the TSM.

For the stiff 5-story building the conclusions are as follows:

- The TSM has been found very sensitive to basis truncation. Results within 10% of the "exact" solution can be obtained from the PFM with a basis of two load-dependent vectors.

8.2.2 Mathematical modelling of viscous damping

Several mathematical models for viscous damping with proportionality coefficients computed from initial elastic properties have been compared to a tangent Rayleigh damping model that kept constant damping ratio throughout the nonlinear analysis. The principal conclusions of this phase of the study are:

- Damping proportional to the instantaneous stiffness with the proportionality coefficients computed from initial elastic properties should be used for MDOF structures with fundamental periods of vibration, T₁ ≤ 0.5 sec to obtain a very good approximation of the more rigorous tangent damping model.
- Rayleigh damping model with constant coefficients based on elastic properties and using the instantaneous stiffness provided a very good agreement with the more rigourous tangent damping model in the medium period range (0.5 < T₁ < 1.5 sec).
- For multistory buildings with T₁ > 1.5 sec, the seismic response is not affected by the type of Rayleigh damping model selected;

The consideration of damping ratios, ξ, of 2% or 5%, force reduction factors, R, of 2 or
 4, and strain hardening ratios, α, of 1% or 25% have no effects on the above conclusions.

8.3 RECOMMENDATIONS FOR FURTHER STUDIES

The present study has raised several points that might be considered in further investigations such as:

- The investigation of the effects of other nonlinearities such as the P-∆ effect and structural pounding on the performance of the PFM and TSM and related energy response.
- The investigation of the effects of other hysteretic model such as the stiffness degrading model or slip model on the performance of the PFM and TSM and related energy response.
- The study of the applicability of the TSM to more complex structures.
- The development and calibration of new damage indices based on tangent properties, power, and energy consideration.
- The investigation of nonlinear behaviour such as force reduction factor from elastic response using the evolution of tangent modal properties.
- The investigation of the effects of numerical damping provided by different integration methods on the energy balance.
- The study of the influence of the adjustment of equivalent damping ratios with the current stress-strain state.
- The investigation of some form of correction based on steady-state frequency domain analysis with low damping response to correct for the incompatibility of updated vector basis in the TSM.

REFERENCES

Bathe, K.J. and Cimento, A.P. (1980). Some Practical Procedures for the Solution of Nonlinear Finite Element Equations, Computer Methods in Applied Mechanics and Engineering, 22, 59-85.

Bathe, K.-J. and Gracewski S. (1981). *On Nonlinear Dynamic Analysis Using Substructuring and Mode Superposition*, Computers & Structures, 13, 699-707.

Chang, C.J. and Mohraz, B. (1990). "Modal Analysis of Nonlinear Systems With Classical and Non-Classical Damping", Computers & Structures, 36, 1067-1080.

Claret, A.M. and Venâncio-Filho, F. (1991). *A modal superposition pseudo-force method for dynamic analysis of structural systems with non-proportional damping*, Earthquake Engineering and Structural Dynamics, 20, 303-315.

Clough, R.W. and Wilson, E.L. (1979). Dynamic Analysis of Large Structural Systems with Local Nonlinearities, Computer Methods in Applied Mechanics and Engineering, 17/18, 107-129.

Conte, J.P., Pister, K.S. and Mahin, S.A. (1990). *Influence of the Earthquake Ground Motion Process and Structural Properties on Response Characteristics of Simple Structures*, Report No. UBC/EERC-90/09, Earthquake Engineering Research Center, University of California, Berkeley.

DiPasquale, E., Ju, J.-W., Askar, A. and Cakmak, A.S. (1990). "Relation Between Global Damage Indices and Local Stiffness Degradation", Journal of Structural Engineering, 116, 1440-1456.

Dungar, R. (1982). 'An imposed force summation method for non-linear dynamic analysis', Earthquake Engineering and Structural Dynamics, 10, 165-170.

El-Aidi, B., and Hall, J.F. (1989). "Nonlinear earthquake response of concrete gravity dams Part 1: modeling.", Earthquake Engineering and Structural Dynamics, 18, 837-851.

Fajfar, P., Fischinger M. and Vidic, T. (1989). *Inelastic Modeling and Seismic Energy Dissipation*, Journal of Structural Engineering, ASCE, 115, 1279-1283.

Fajfar, P. and Fischinger, M. (1990). "Earthquake Design Spectra Considering Duration of Ground Motion", Proceedings of Fourth U.S. National Conference on Earthquake Engineering, EERI, 2, 15-24.

Filho, F.V., Coutinho, A.L.G.A., Landau, L., Lima, E.C.P. and Ebecken, N.F.F. (1988). "Nonlinear Dynamic Analysis Using the Pseudo-Force Method and the Lanczos Algorithm", Computers & Structures, 30, 979-983.

Filiatrault, A. (1990). *Static and Dynamic Analysis of Timber Shear Walls*, Canadian Journal of Civil Engineering, 17, 643-651.

Geschwindner, L.F. (1981). *Nonlinear dynamic analysis by modal superposition*, Journal of Structural Engineering, ASCE, 107, 2325-2336.

Gillies, A.G. and Shepherd, R. (1983). "Prediction of Post-Elastic Seismic Response of Structures by a Mode Superposition Technique", Bulletin of the New Zealand National Society for Earthquake Engineering, 16, 222-233.

Hadidi-Tamjed, H. (1988). "Statistical Response of Inelastic SDOF Systems Sybjected to Earthquakes", Ph.D. Thesis, Stanford University, California.

Hanna, M.M. (1989). "An Efficient Mode Superposition Method for the Numerical Dynamic Analysis of Bilinear Systems", Ph.D. Thesis, University of California, Irvine

Hofmeister, L.D. (1978). "Dynamic Analysis of Structures Containing Nonlinear Springs", Computers & Structures, 8, 609-614.

Housener, G.W., and Jennings, P.C. (1977). 'The capacity of extreme earthquake motions to damage structures.' Structural and Geotechnical Mechanics, W.J. Hall, ed. Prentice-Hall, Inc., Englewood Cliffs, N.J., 102-116.

Ibrahimbegovic, A. and Wilson, E.L. (1989). "Simple Numerical Algorithms for the Mode Superposition Analysis of Linear Structural Systems with Non-Proportional Damping", Computers & Structures, 33, 523-531.

Ibrahimbegovic, A. and Wilson, E.L. (1990). "A Methodology for Dynamic Analysis of Linear Structure-Foundation Systems with Local Non-Linearities", Earthquake Engineering and Structural Dynamics, 19, 1197-1208.

Idelsohn, S.R. and Cardona, A. (1985). A Load-Dependent Basis for Reduced Nonlinear Structural Dynamics, Computers & Structures, 20, 203-210.

Idelsohn, S.R. and Cardona, A. (1985). A Reduction Method for Nonlinear Structural Dynamic Analysis, Computer Methods in Applied Mechanics and Engineering, 49, 253-279

Kannan, A.E., and Powell, G.H. (1973). *DRAIN-2D a general purpose computer program for dynamic analysis of inelastic plane structures*, Report No. UBC/EERC-73/6 and 73/22, Earthquake Engrg. Res. Ctr., Univ. of California, Berkeley.

Knight, N. (1985). Nonlinear structural dynamic analysis using a modified modal method', AIAA Journal, 23, 1594-1601.

Kuwamura, H. and Galambos, T.V. (1989). *Earthquake Load for Structural Reliability*, Journal of Structural Engineering, ASCE, 115, 1446-1462.

Léger, P. and Wilson, E.L. (1987). *Generation of Load Dependent Ritz Transformation Vectors in Structural Dynamics*, Engineering Computations, 4, 309-318.

Léger, P. and Wilson, E.L. (1988). *Modal Summation Methods for Structural Dynamic Computations*, Earthquake Engineering and Structural Dynamics, 16, 23-27.

Lin, J. and Mahin, S.A. (1985). *Effect of Inelastic Behavior on the Analysis and Design of Earthquake Resistant Structures*, Report No. UBC/EERC-85/08, Earthquake Engineering Research Center, University of California, Berkeley.

Lukkunaprasit, P., Widartawan, S. and Karasudhi, P. (1980). "Dynamic Response of an Elastic-Viscoplastic System in Modal Coordinates", Earthquake Engineering and Structural Dynamics, 8, 237-250.

McCabe, S.L. and Hall, W.J. (1989). "Assessment of Seismic Structural Damage", Journal of Structural Engineering, ASCE, 115, 2166-2183.

Maison, B.F. and Kasai, K. (1990). *Analysis for Type of Structural Pounding*, Journal of Structural Engineering, ASCE, 116, 957-977.

Molnar, A.J., Vashi, K.M., and Say, C.W. (1976). "Application of normal mode theory and pseudo-force methods to solve problems with nonlinearities", ASME Journal of Pressure Vessel Technology, 151-156.

Morris, N.F. (1977). 'The Use of Modal Superposition in Nonlinear Dynamics', Computers & Structures, 7, 65-72.

Muscolino, G. (1989). *Mode-superposition methods for elastoplastic systems*, Journal of Engineering Mechanics, ASCE, 115, 2199-2215.

National Building Code of Canada 1990, (1990). Associate Committee on the National Building Code, National Reasearch Council of Canada, Ottawa.

Nickell, R.E. (1976). Nonlinear Dynamics by Mode Superposition, Computer Methods in Applied Mechanics and Engineering, 7, 107-129.

Noor, A.K. (1981). "Recent Advances in Reduction Methods for Nonlinear Problems", Computers & Structures, 13, 31-44.

Otani, S. (1980). "Nonlinear dynamic analysis of reinforced concrete building structures", Canadian Journal of Civil Engineering, 7, 333-344.

Pall, A.S., and Marsh, C. (1982). "Response of friction damped braced frames", Journal of Structural Engineering, ASCE, 1313-1323.

Remseth, S.N. (1979). "Nonlinear Static and Dynamic Analysis of Framed Structures", Computers & Structures, 10, 879-897.

Schiff, S.D. (1988). *Seismic Design Studies of Low-Rise Steel Frames*, Ph D. Thesis, University of Illinois, Urbana-Champaign.

Schiff, S.D., Hall, W.D. and Foutch, D.A. (1991). *Seismic Performance of Low-Rise Steel Perimeter Frames*, Journal of Structural Engineering, ASCE, 117, 546-562.

Shah, V.N., Bohm, G.J. and Nahavandi, A.N. (1979). "Modal Superposition Method for Computationally Economical Nonlinear Structural Analysis", Journal of Pressure Vessel Technology, 101, 134-141.

Stricklin, J.A. and Haisler, W.E. (1977). *Formulations and Solution Procedures for Nonlinear Structural Analysis*, Computers & Structures, 7, 125-136.

Tembulkar, J.M. and Nau, J.M. (1987). "Inelastic Modeling and Seismic Energy Dissipation", Journal of Structural Engineering, ASCE, 113, 1373-1377.

Uang, C.-M. and Bertero, V.V. (1990). 'Evaluation of Seismic Energy in Structures', Earthquake Engineering and Structural Dynamics, 19, 77-90.

Uang, C.-M. (1991). *Establishing R (or R_w) and C_D Factors for Building Seismic Provisions*, Journal of Structural Engineering, ASCE, 117, 19-28.

Udwadia, F.E. and Esfandian, S. (1990). Non-Classically Damped Dynamic Systems: an Iterative Approach, Journal of Applied Mechanics, 57, 423-433.

Villaverde, R. (1988). *Modal superposition method for seismic design of non-linear multistory structures*, Earthquake Engineering and Structural Dynamics, 16, 691-704

Wilson, E.L., Yuan, M.W. and Dickens, J.M. (1982) *Dynamic analysis by direct superposition of Ritz vectors*, Earthquake Engineering and Structural Dynamics, 10, 813-824.

Wu, J. and Hanson, R.D. (1989). "Study of Inelastic Spectra with High Damping", Journal of Structural Engineering, ASCE, 115, 1412-1431.

Zahrah, T.F. and Hall, W.J. (1984). "Earthquake Energy Absorption in SDOF Structures", Journal of Structural Engineering, ASCE, 110, 1757-1772.